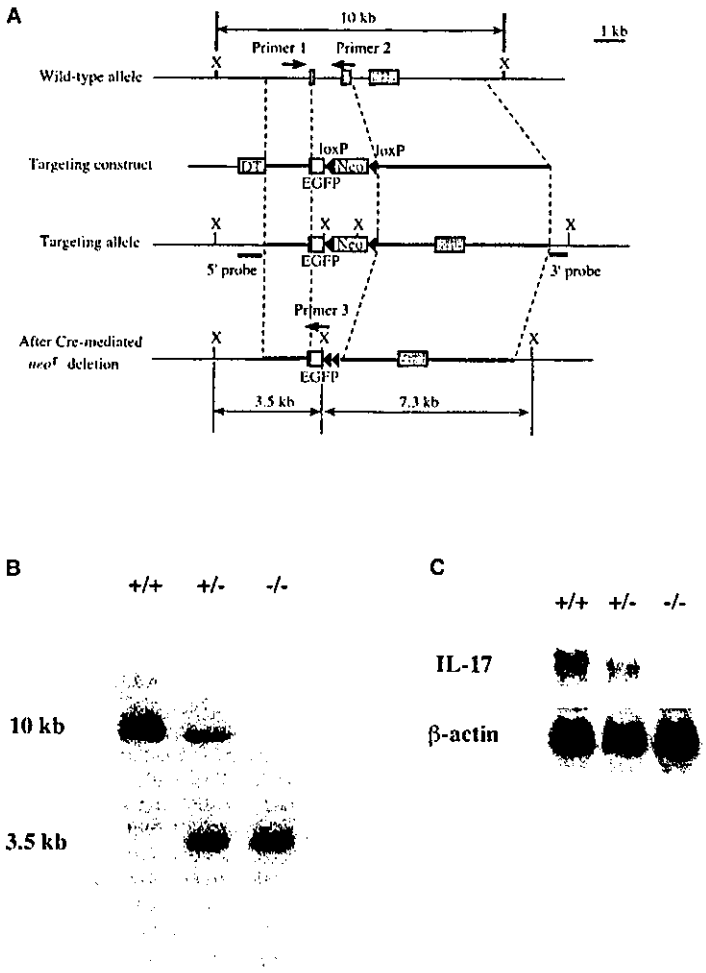

Figure 1. Generation of IL-17$^{-/-}$ Mice

(A) Structure of the mouse *il-17* locus (Wild-type allele), the IL-17 targeting construct (Targeting construct), and the predicted mutated *il-17* gene before (Targeting allele) and after neomycin resistance gene (*neo*^{r}) deletion (After Cre-mediated *neo*^{r} deletion). Exons are represented by boxes. Exon 1 and 2 of the *il-17* gene were replaced with the *EGFP* gene and the *neo*^{r} gene flanked by lox P sequences. A *DT* gene was attached to the 5' end of the genomic fragment for negative selection. The external homologous regions shown in the targeting allele were used as the genomic probe for Southern blot analysis. Southern blot analysis for targeted clone screening was carried out using XbaI (X). Primers 1, 2, and 3 were used for genotyping of mice.

(B) Southern blot analysis of the thymus DNA from IL-17 wild-type (+/+), heterozygous (+/−), and mutant (−/−) littermates. The endogenous (10 kb) and targeted (3.5 kb) bands were shown using the 5' probe.

(C) Northern blot analysis of the IL-17 mRNA from splenic T cells stimulated with plate-coated anti-CD3 plus anti-CD28 mAb for 48 hr.

sitivity response (AHR), but not in acute graft-versus-host reaction (GVHR), through activation of T cell priming.

Results

Generation of IL-17-Deficient Mice

We generated IL-17$^{-/-}$ mice by replacing the exon 1 and 2 of the *il-17* gene with a neomycin resistance gene (Figure 1A). Correct targeting of the IL-17 locus was confirmed by genomic Southern blot analysis (Figure 1B). The expression of IL-17 mRNA was not detected by Northern blot analysis in splenic T cells from IL-17$^{-/-}$ mice stimulated with plate-coated anti-CD3 plus anti-CD28 mAb (Figure 1C). The levels of IL-17 protein in the supernatant from IL-17$^{-/-}$ T cell cultures were below the limit of detection by ELISA (Figure 2C).

IL-17$^{-/-}$ mice were generated from the cross between IL-17$^{+/-}$ mice at the expected Mendelian ratio. They were fertile and did not show any gross phenotypic abnormalities under specific pathogen-free housing conditions (data not shown). No apparent abnormalities were found in the cell populations of the thymus, LNs, and spleen among IL-17$^{+/+}$, IL-17$^{+/-}$, and IL-17$^{-/-}$ mice (data not shown).

T Cell Response to Mitogenic Stimuli

IL-17 is known as a T cell costimulatory factor (Yao et al., 1995a). To examine whether IL-17 is necessary for T cell activation, splenic T cells from IL-17$^{-/-}$ mice were stimulated with plate-coated anti-CD3 plus anti-CD28 mAb. Proliferative responses of IL-17$^{-/-}$ T cells and IL-4 and IFN-γ production were normal (Figures 2A and 2B), although IL-17 production was completely abolished (Figure 2C). Proliferative responses of whole spleen cells to other mitogenic stimuli such as ConA, PHA, and PMA plus ionomycin were also shown to be normal in IL-17$^{-/-}$ mice (Figure 2D). Therefore, these results indicate that IL-17 is not necessary for either cell proliferation or IL-4 or IFN-γ production by T cells in response to nonspecific mitogenic stimuli.

CHS

It was shown that nickel-specific skin-derived T cells produce IL-17, and this IL-17 induces IL-6 and IL-8 production as well as ICAM-1 and HLA-DR expression on

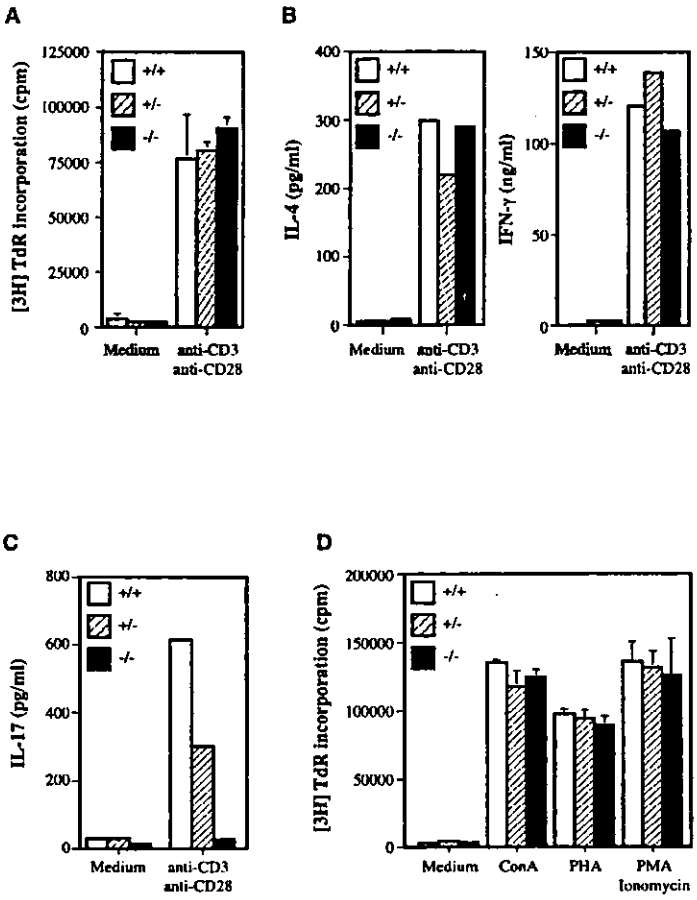

Figure 2. T Cell Functions of IL-17$^{-/-}$ Mice

Splenic T cells (A, B, and C) and whole spleen cells (D) from IL-17$^{+/+}$, IL-17$^{+/-}$, and IL-17$^{-/-}$ mice were stimulated with mitogenic stimuli. Proliferative responses (A), IL-4 and IFN-γ levels (B), and IL-17 levels (C) in the culture supernatants are shown after stimulation with plate-coated anti-CD3 plus anti-CD28 mAb for 48 hr, and proliferative responses to mitogens after 48 hr are shown in (D). Average ± SD of three wells is shown in the proliferation assay, and cytokine levels in pooled supernatant from three wells were determined by ELISA. These results were reproducible in two independent experiments.

keratinocytes in humans (Albanesi et al., 1999). To elucidate the role of IL-17 in hapten-specific skin diseases, we investigated CHS responses in IL-17$^{-/-}$ mice. DNFB- and TNCB-induced CHS responses in IL-17$^{-/-}$ mice were markedly suppressed compared with those in IL-17$^{+/+}$ mice (Figures 3A and 3B). The response in IL-17$^{+/-}$ mice was similar to that in IL-17$^{+/+}$ mice (data not shown). IL-17$^{+/+}$ mice exhibited infiltration of a large number of inflammatory cells into the TNCB-challenged ear epidermis, while cell infiltration was not shown in vehicle-treated ears (Figure 3C). In contrast, inflammatory cell infiltration in TNCB-treated ears was markedly reduced in IL-17$^{-/-}$ mice (Figure 3C).

IL-17 is known to enhance T cell activation via promotion of DC maturation (Antonysamy et al., 1999). Langerhans cells (LCs), which are the major antigen-presenting cells in CHS response, are immature in the skin and maturate during the migration process from the skin to draining LNs after activation with antigens (Grabbe and Schwarz, 1998). However, LC migrating into draining LNs from the skin expressed normally cell surface activation markers, CD40 and CD86, in IL-17$^{-/-}$ mice after painting with FITC on the skin (Figure 3D). Six hours after LPS stimulation, IL-12 expression in FITC^{+}CD11c^{+} LCs was also comparable between IL-17$^{+/+}$ and IL-17$^{-/-}$ mice (Figure 3D). When T cells from DNFB-sensitized IL-17$^{-/-}$ mice were cocultured with CD11c^{+} DCs from IL-17$^{+/+}$ or IL-17$^{-/-}$ mice in the absence or presence of DNBS, IL-17$^{-/-}$ DCs could promote T cell proliferation in a manner similar to IL-17$^{+/+}$ DCs (Figure 3E). Furthermore, when nontreated IL-17$^{-/-}$ mice were injected with TNP-conjugated splenic DCs from IL-17$^{+/+}$ or IL-17$^{-/-}$ mice, the severity of CHS in mice that received IL-17$^{-/-}$ DCs was similar to that in IL-17$^{-/-}$ mice that received IL-17$^{+/+}$ DCs (Figure 3F). Thus, these results indicate that IL-17 deficiency does not affect LC/DC function during CHS response. On the other hand, TNP- and DNP-specific T cell proliferative responses from draining LNs of IL-17$^{-/-}$ mice were significantly decreased compared with those of IL-17$^{+/+}$ mice (Figures 3G and 3H). Among CD3^{+} cells, CD4^{+} T cells but not CD8^{+} T cells showed reduced proliferative response against DNBS (Figure 3I). IFN-γ production after stimulation with DNBS was markedly reduced in the IL-17$^{-/-}$ T cell culture, while IL-4 production was almost undetectable both in the IL-17$^{+/+}$ T cell and the IL-17$^{-/-}$ T cell cultures (Figure 3H). When TNCB-sensitized T cells were transferred into nontreated mice, the CHS response in mice that received T cells from IL-17$^{-/-}$ mice was significantly lower compared with the response in mice that received T cells from IL-17$^{+/+}$ mice (Figure 3J). However, when IL-17$^{-/-}$ mice were previously transplanted with CD4^{+} T

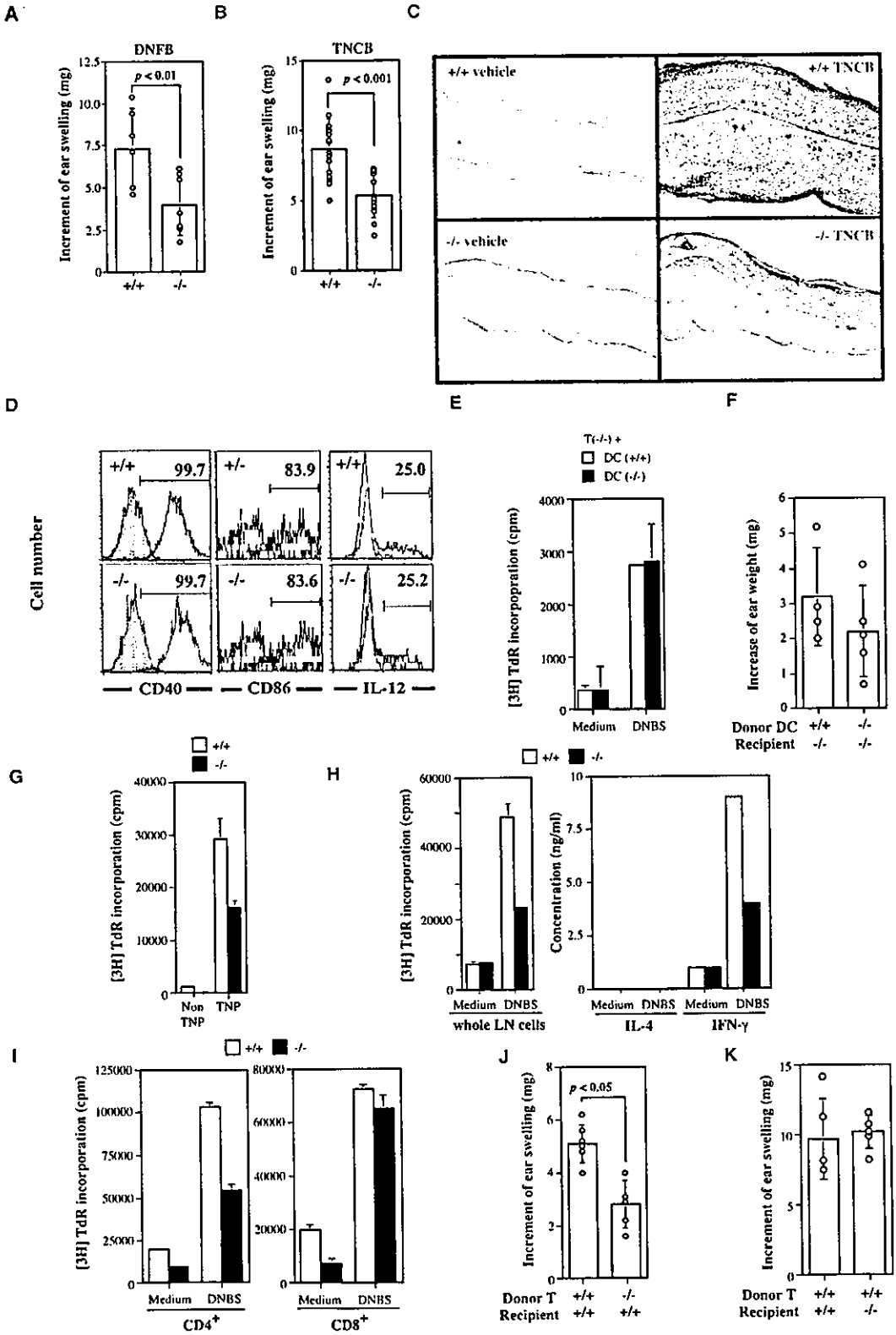
A
DNFB
p < 0.01
Increment of ear swelling (mg)
+/+
-/-
B
TNCB
p < 0.001
Increment of ear swelling (mg)
+/+
-/-
C
+/+ vehicle
+/+ TNCB
-/- vehicle
-/- TNCB
D
Cell number
+/+ 99.7
+/- 83.9
+/+ 25.0
-/- 99.7
-/- 83.6
-/- 25.2
CD40
CD86
IL-12
E
T(-/-) +
DC (+/+)
DC (-/-)
[3H] TdR incorpopration (cpm)
Medium
DNBS
F
Increase of ear weight (mg)
Donor DC +/+ -/-
Recipient -/- -/-
G
+/+
-/-
[3H] TdR incorporation (cpm)
Non TNP
TNP
H
+/+
-/-
[3H] TdR incorporation (cpm)
Medium DNBS
whole LN cells
Concentration (ng/ml)
Medium DNBS
IL-4
Medium DNBS
IFN-γ
I
+/+
-/-
[3H] TdR incorporation (cpm)
Medium DNBS
CD4+
Medium DNBS
CD8+
J
p < 0.05
Increment of ear swelling (mg)
Donor T +/+ -/-
Recipient +/+ +/+
K
Increment of ear swelling (mg)
Donor T +/+ +/+
Recipient +/+ -/-

cells from wild-type mice before sensitization, CHS in these reconstituted mice was recovered to the levels of wild-type mice (Figure 3K). Therefore, these results indicate that IL-17 is required for hapten-specific T cell activation, especially for $CD4^+$ T cells, but not for LC maturation in the sensitization phase of CHS response.

To elucidate the effects of IL-17 deficiency on humoral immunity, TNP-specific Ig levels in sera from IL-$17^{-/-}$ mice at 3 days after TNCB challenge were determined by ELISA. All TNP-specific IgG subclass levels in sera from IL-$17^{-/-}$ mice were significantly lower compared with those from IL-$17^{+/+}$ mice (Figure 4A). Thus, we showed that IL-17 also plays an important role in humoral immunity.

In the elicitation phase of CHS, various cells such as neutrophils, macrophages, and T cells were seen to have infiltrated the sites which were chemically challenged. In this phase, vascular permeability is important for cellular infiltration. Because of this, we investigated the vascular permeability of IL-$17^{-/-}$ mice, since IL-17 is thought to be involved in this process through the induction of *iNOS* and *cox-2* (Shalom-Barak et al., 1998). One hour after a TNCB challenge, exudation of Evans blue dye in the ear was normal in IL-$17^{-/-}$ mice (Figure 4B).

To assess the effect of IL-17 deficiency on the expression of proinflammatory cytokines, chemokines, and cell adhesion molecules, protein and mRNA levels were analyzed by ELISA and Northern blot hybridization analysis, respectively. IL-1α, IL-1β, and TNF-α levels in the lysate of the IL-$17^{-/-}$ mouse ears challenged with TNCB were similar to those of IL-$17^{+/+}$ mice. In addition, these cytokines were produced with similar kinetics (Figures 4C and 4D), although IL-17 was not produced in IL-$17^{-/-}$ mice (Figure 4C). On the other hand, the mRNA levels of chemokines were reduced by 20%–50% in IL-$17^{-/-}$ mice compared with IL-$17^{+/+}$ mice at 6 hr after TNCB challenge (Figure 4E). ICAM-1 expression also decreased partially in IL-$17^{-/-}$ mice (Figure 4E).

The level of neutrophil infiltration was estimated by MPO assay (Figure 4F). The results showed the involvement of IL-17 in this process, consistent with the results of a previous report (Fossiez et al., 1998) and with the finding that the expression of chemokine mRNAs for Groα, MIP-1, and MIP-2 were found to be reduced (Figure 4E). These results show that IL-17 also plays an important role in the infiltration process of inflammatory cells.

It is known that TNF-α is also involved in CHS response, and it was reported recently that IL-17 was expressed by T cells producing TNF-α (Infante-Duarte et al., 2000). We then examined whether or not the role of IL-17 in CHS response was different from that of TNF-α. TNF-α production in the inflammatory sites was normal in IL-$17^{-/-}$ mice, and IL-17 production on T cells of TNF-$\alpha^{-/-}$ mice was also found to be normal (data not shown). CHS responses in TNF-$\alpha^{-/-}$ mice as well as in IL-$17^{-/-}$ mice were similarly reduced compared with those in wild-type mice, and those in IL-$17^{-/-}$ x TNF-$\alpha^{-/-}$ mice were severely reduced compared with those in TNF-$\alpha^{-/-}$ or in IL-$17^{-/-}$ mice (Figure 4G).

These results suggest that the reduced CHS response in IL-$17^{-/-}$ mice is caused by a TNF-α-independent mechanism. Taken together, these results indicate that IL-17 has an important role in hapten-specific cellular and humoral immunities during CHS response.

DTH

We examined the role of IL-17 in the DTH response, which is a Th1 cell-mediated cellular immune response. Methylated-BSA (mBSA)-induced DTH response in IL-$17^{-/-}$ mice was suppressed to approximately 80% of the average response in IL-$17^{+/+}$ mice (Figure 5A). In IL-$17^{-/-}$ mice, cell infiltration at the inflammatory site was milder than in IL-$17^{+/+}$ mice (data not shown). The T cell proliferative response of IL-$17^{-/-}$ mice against mBSA was reduced compared with those of IL-$17^{+/+}$ mice (Figure 5B). Consistent with the proliferation levels, IFN-γ production in culture supernatants from IL-$17^{-/-}$ mice was also found to be lower than that from IL-$17^{+/+}$ mice (Figure 5C). IL-4 levels were below the level of detection

Figure 3. Impaired CHS Response in IL-$17^{-/-}$ Mice

(A) Increase of ear swelling in DNFB-induced CHS 24 hr after the second challenge.

(B) Increase of ear swelling in TNCB-induced CHS 24 hr after the second challenge.

(C) Histology of the ear skin at 24 hr after the challenge with TNCB or vehicle alone. Hematoxylin-eosin staining, ×40.

(D) CD40, CD86, and IL-12 expression on $CD11c^+$ $FITC^+$ LCs. The expression of activation marker on LCs migrating into draining LNs from the skin 24 hr after FITC painting was analyzed by FACS. For IL-12 expression, draining LNs from the skin 24 hr after painting with FITC were stimulated with 10 μg/ml LPS plus 2 μM monensin for 6 hr. Shaded area shows an isotype-matched control Ig staining.

(E) Antigen presentation ability of IL-$17^{-/-}$ DCs. DNFB-sensitized IL-$17^{-/-}$ T cells (5×10^4 cells) were cocultured with DCs from IL-$17^{+/+}$ or IL-$17^{-/-}$ mice in the absence or presence of 25 μg/ml DNBS for 3 days, and then [^{3}H] TdR incorporation was measured.

(F) CHS response after adoptive transfer of DCs. $CD11c^+$ splenic DCs were purified from IL-$17^{+/+}$ or IL-$17^{-/-}$ mice and treated with TNBS. Then, the TNP-conjugated DCs were transferred into IL-$17^{-/-}$ recipient mice, and CHS was measured after challenging with TNCB.

(G) Reduced TNP-specific T cell proliferation response in IL-$17^{-/-}$ mice. Inguinal and axillary LN T cells were purified from IL-$17^{+/+}$ or IL-$17^{-/-}$ mice sensitized with TNCB 5 days after the first challenge and were cocultured with TNBS-treated splenic adherent cells for 3 days.

(H) DNP-specific T cell proliferative responses and IL-4 and IFN-γ production. Inguinal and axillary LN cells from IL-$17^{+/+}$ or IL-$17^{-/-}$ mice sensitized with DNFB were harvested 5 days after the first challenge and cultured in the absence or presence of 50 μg/ml DNBS for 3 days.

(I) Inguinal and axillary LN $CD4^+$ or $CD8^+$ cells from IL-$17^{+/+}$ or IL-$17^{-/-}$ mice sensitized with DNFB were cocultured with splenic adherent cells in the absence or presence of 50 μg/ml DNBS for 3 days.

(J) CHS response after adoptive transfer of T cells. Inguinal and axillary LN T cells from TNCB-sensitized IL-$17^{+/+}$ or IL-$17^{-/-}$ mice were transferred, and CHS response of the T cell-transferred mice was examined by challenging TNCB on the ear.

(K) Reconstitution of IL-$17^{-/-}$ mice with IL-$17^{+/+}$ $CD4^+$ T cells. $CD4^+$ T cells (4×10^7 cells) were purified from IL-$17^{+/+}$ mice, and they were injected into naive IL-$17^{+/+}$ or IL-$17^{-/-}$ mice. Then, these mice were sensitized with TNCB, and CHS was measured.

(A, B, F, J, and K) Each circle represents an individual mouse, and average and SD are shown. (E, G, H, and I) Average ± SD of three wells is shown in the proliferation assay, and cytokine levels in a pooled supernatant from three wells from proliferative response assay were determined by ELISA. These results were reproducible in at least three independent experiments.

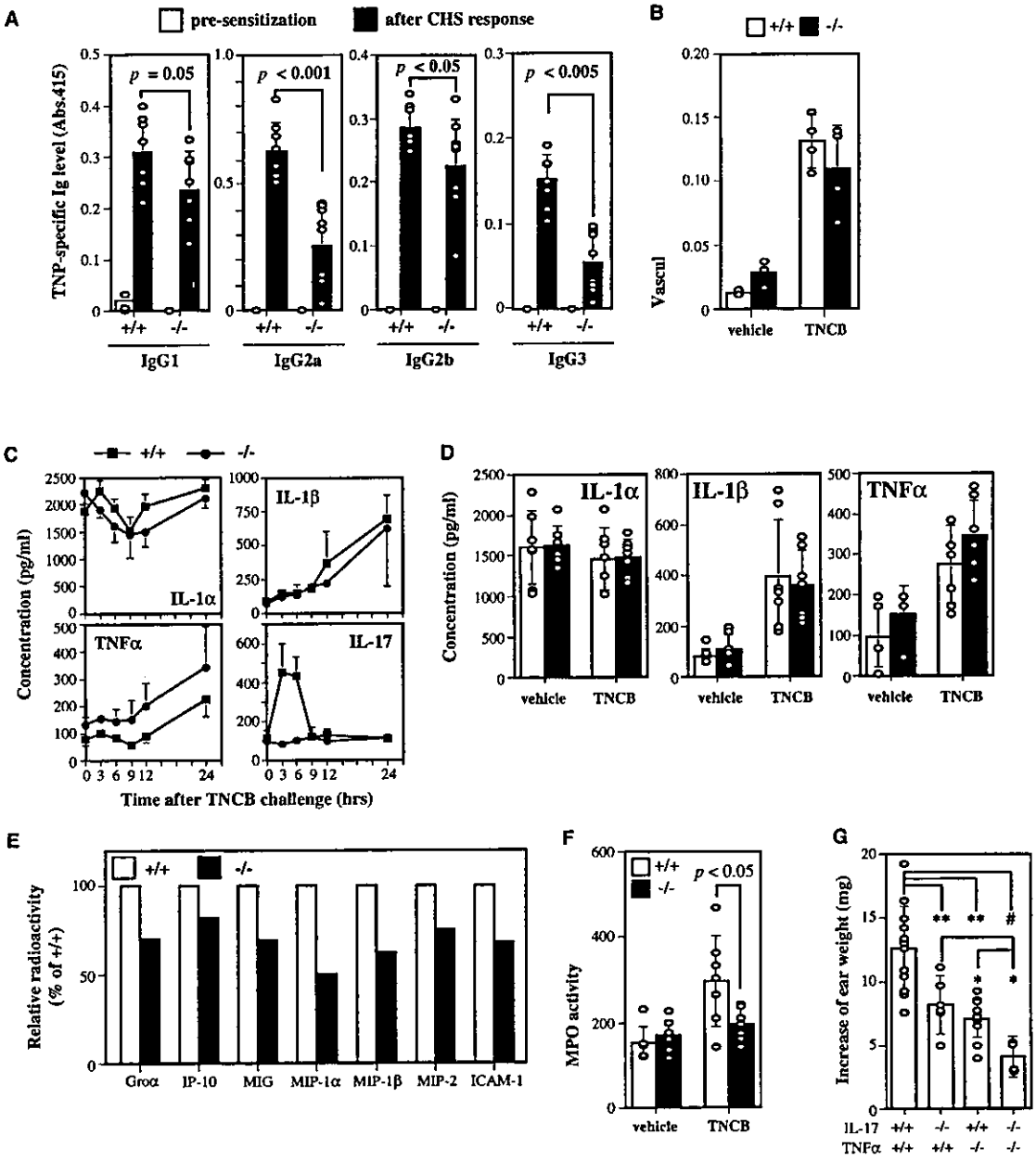

Figure 4. Impaired CHS Response in IL-17$^{-/-}$ Mice

(A) TNP-specific antibody production during CHS response. Three days after the challenge with TNCB, sera were collected and antibody levels were measured by ELISA.

(B) Vascular permeability in CHS response. Evans blue dye was injected intravenously after the challenge with TNCB, and 1 hr later, exudative dye in the ear skin was extracted, and the absorbancy at 650 nm was measured.

(C) IL-1α, IL-1β, TNF-α, and IL-17 levels in the ear after challenge with TNCB. The ears were removed at the time indicated after the second challenge, and cytokine levels in the lysate were measured by ELISA. The average of three mice is shown.

(D) IL-1α, IL-1β, and TNF-α levels in the lysate of the ear challenged with TNCB. Cytokine levels were measured by ELISA 24 hr after the challenge.

(E) Northern blot analysis of the mRNAs of chemokines and an adhesion molecule in the ear skin at 6 hr after the challenge with TNCB. β-actin mRNA was used to normalize the amount of loaded RNA, and the relative values in IL-17$^{-/-}$ mice compared to those in IL-17$^{+/+}$ mice are shown.

(F) MPO activity in CHS response. The lysate of the ear skin was prepared at 24 hr after the challenge with TNCB, and MPO activity was measured.

(G) TNCB-induced CHS responses in IL-17$^{-/-}$, TNF-α$^{-/-}$, and IL-17$^{-/-}$ x TNF-α $^{-/-}$ mice.

(A, B, D, F, and G) Each circle represents an individual mouse, and average and SD are shown. $p < 0.05$; **, $p < 0.01$; #, $p < 0.005$.

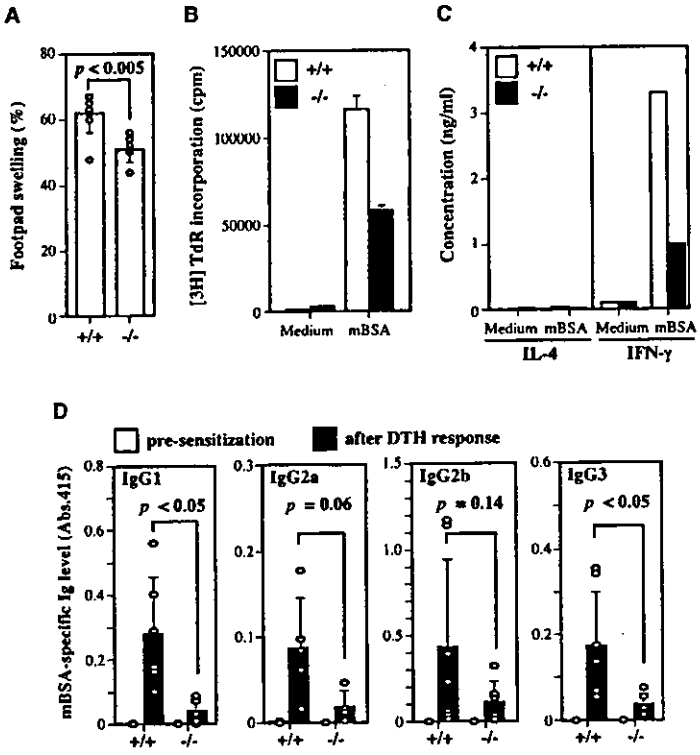

Figure 5. Impaired DTH Response in IL-17$^{-/-}$ Mice

(A) Increase of footpad thickness in mBSA-induced DTH response. Each circle represents an individual mouse, and average and SD are shown.

(B) mBSA-specific T cell proliferative response. Inguinal LN cells from IL-17$^{+/+}$ or IL-17$^{-/-}$ mice sensitized with mBSA/CFA subcutaneously for 1 week were cultured in the absence or presence of 40 μg/ml mBSA for 3 days. The average ± SD of three wells is shown. These results were reproducible in three independent experiments.

(C) IL-4 and IFN-γ levels in the pooled supernatant of three wells from proliferative response assay were determined by ELISA. These results were reproducible in three independent experiments.

(D) mBSA-specific antibody levels after DTH reaction. One week after the challenge with mBSA, sera were collected, and mBSA-specific antibody levels were measured. Each circle represents an individual mouse, and average and SD are shown.

in both IL-17$^{+/+}$ and IL-17$^{-/-}$ culture supernatants (Figure 5C). One week after the DTH response, mBSA-specific IgG1 and IgG3 levels in sera from IL-17$^{-/-}$ mice were significantly reduced compared with those in IL-17$^{+/+}$ mice (Figure 5D). These results indicate that IL-17 also plays an important role in the induction of the Th1-mediated DTH response.

AHR

IL-17 is found in the sera of allergic asthma patients (Wong et al., 2001). In order to assess whether or not IL-17 is involved in the development of asthma, we analyzed OVA/alum-induced AHR using IL-17$^{-/-}$ mice. Five days after the first immunization with OVA/alum intraperitoneally, the proliferative response of the mesenteric LN cells from IL-17$^{-/-}$ mice against OVA was markedly reduced compared with that of the IL-17$^{+/+}$ mice (Figure 6A). IL-4 and IL-5 levels in the supernatant of IL-17$^{-/-}$ LN cell cultures were also lower than those of IL-17$^{+/+}$ LN cell cultures, while IFN-γ levels of both IL-17$^{+/+}$ and IL-17$^{-/-}$ LN cell cultures were similar (Figure 6B).

Furthermore, when mice were immunized with OVA/alum intraperitoneally, OVA-specific IgG1 and IgE levels in IL-17$^{-/-}$ mice were significantly reduced compared with those in IL-17$^{+/+}$ mice (Figure 6C). In spite of the reduced OVA-specific T cell responses, the AHR to methacholine in IL-17$^{-/-}$ mice were similar to those of IL-17$^{+/+}$ and IL-17$^{+/-}$ mice (Figure 6D).

The total infiltrated cell numbers in bronchoalveolar lavage fluids (BALF) (Figure 6E) and the pulmonary pathology (data not shown) were not different between the IL-17$^{+/+}$, IL-17$^{+/-}$, and IL-17$^{-/-}$ mice. Moreover, IL-4 and IL-5 levels in the BALF from IL-17$^{-/-}$ mice at 24 hr after the last inhalation with OVA were higher than those from IL-17$^{+/+}$ and IL-17$^{+/-}$ mice (data not shown). The apparent discrepancy between the reduced T cell activation and normal AHR with pulmonary inflammation in IL-17$^{-/-}$ mice may be explained by the effect of alum, which induces an excess Th2 response independently from IL-4 and IL-13 signaling (Brewer et al., 1999).

We then examined the role of IL-17 in OVA-induced AHR without alum using IL-17$^{-/-}$ x DO11.10 transgenic (Tg) mice. Twenty-four hours after the last inhalation with OVA, the AHR to methacholine in IL-17$^{-/-}$ x DO11.10 Tg mice was partially decreased compared with that in IL-17$^{+/-}$ x DO11.10 Tg mice (Figure 6F). Consistent with AHR, the number of total infiltrated cells in BALF from IL-17$^{-/-}$ x DO11.10 Tg mice was reduced compared with that of IL-17$^{+/-}$ x DO11.10 Tg mice (Figure 6G). As expected, pulmonary inflammation in IL-17$^{-/-}$ x DO11.10 Tg mice was also found to be milder than that of IL-17$^{+/-}$ x DO11.10 Tg mice (Figure 6H). These observations indicate that IL-17 is involved in the induction of AHR.

Acute GVHR

We then examined the role of IL-17 in acute GVHR. When splenocytes from IL-17$^{-/-}$ or IL-17$^{+/+}$ mice on the C57BL/6J background (H-2K^{b}) were transferred into CBF1 mice (H-2K$^{b/d}$), the number of IL-17$^{-/-}$ CD4^{+} T cells in the spleen of recipient CBF1 mice was similar to that of IL-17$^{+/+}$ CD4^{+} T cells (Figure 7A). A similar

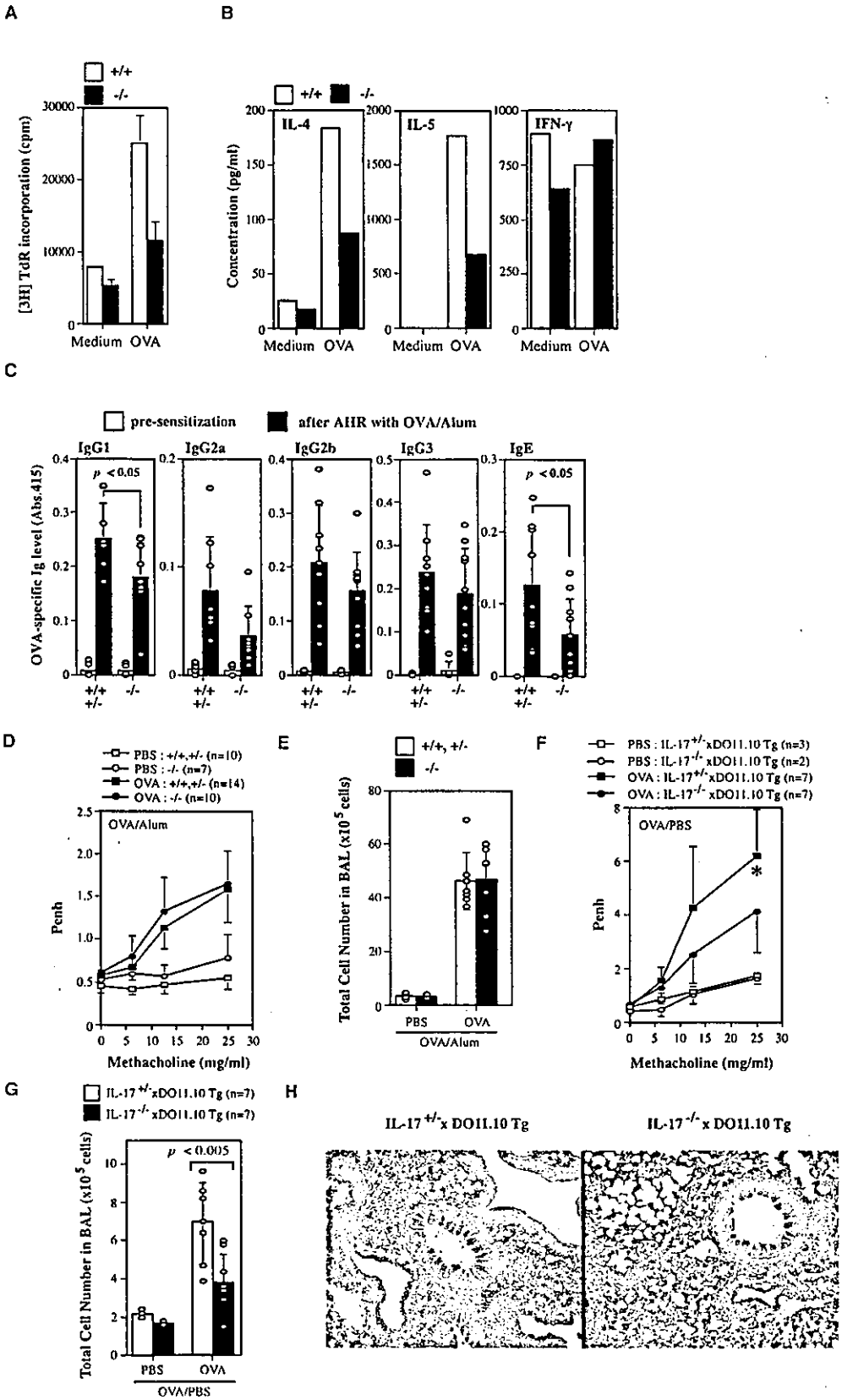
A
B
+/+
-/-
[3H] TdR incorporation (cpm)
Medium OVA
Concentration (pg/ml)
IL-4
IL-5
IFN-γ
C
pre-sensitization
after AHR with OVA/Alum
IgG1
IgG2a
IgG2b
IgG3
IgE
p < 0.05
OVA-specific Ig level (Abs.415)
D
PBS : +/+,+/- (n=10)
PBS : -/- (n=7)
OVA : +/+,+/- (n=14)
OVA : -/- (n=10)
OVA/Alum
Penh
Methacholine (mg/ml)
E
Total Cell Number in BAL (x10^5 cells)
PBS
OVA
F
PBS : IL-17+/- xDO11.10 Tg (n=3)
PBS : IL-17-/- xDO11.10 Tg (n=2)
OVA : IL-17+/- xDO11.10 Tg (n=7)
OVA : IL-17-/- xDO11.10 Tg (n=7)
OVA/PBS
G
IL-17 +/- xDO11.10 Tg (n=7)
IL-17 -/- xDO11.10 Tg (n=7)
p < 0.005
H
IL-17 +/- x DO11.10 Tg
IL-17 -/- x DO11.10 Tg

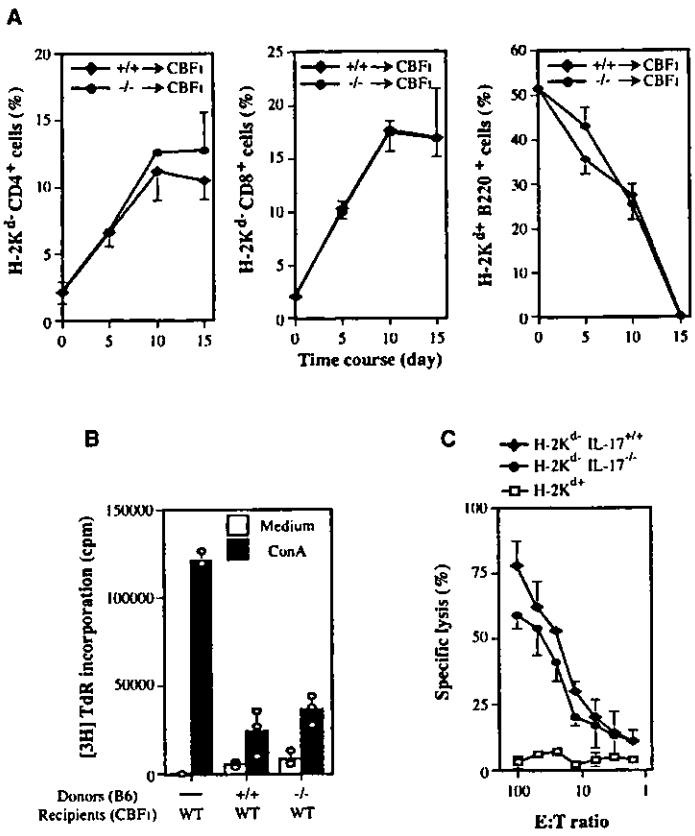

Figure 7. Normal Acute GVHR by IL-17$^{-/-}$ Donor Cells

Spleen cells from IL-17$^{+/+}$ or IL-17$^{-/-}$ mice on the C57BL/6J background (H-2K$^{b/b}$) were transferred into CBF1 (C57BL/6J x BALB/cA F1: H-2K$^{b/d}$) mice intravenously.

(A) At indicated time points after the transfer, the spleen of the recipient CBF1 mice was removed, and the expansion of H-2K^{d-}CD4$^+$ or H-2K^{d-}CD8$^+$ cells of the donor IL-17$^{+/+}$ or IL-17$^{-/-}$ spleen cells and the reduction of H-2K^{d+}B220$^+$ cells of the recipient CBF1 mice were analyzed by FACS. Symbols represent the average of three mice and SD.

(B) Proliferative responses of the recipient CBF1 spleen cells to ConA at 10 days after transfer. Each circle represents an individual mouse, and average and SD are shown.

(C) CTL activity to P815 cells (H-2K^{d+}). Ten days after the transfer, H-2K^{d-}CD8$^+$ T cells were purified from the recipient CBF1 spleen cells by the MACS system. Specific lysis of H-2K^{d+}P815 cells by H-2K^{d-}CD8$^+$ T cells was determined by the ^{51}Cr release assay. Symbols represent the average of three mice and SD.

tendency was also observed in CD8$^+$ T cells from IL-17$^{-/-}$ mice (Figure 7A). The reduction kinetics of the recipient B cells was also similar in mice that received IL-17$^{+/+}$ and IL-17$^{-/-}$ T cells (Figure 7A). The ConA response of the recipient spleen cells from CBF1 mice that received IL-17$^{+/+}$ and IL-17$^{-/-}$ spleen cells was similarly reduced (Figure 7B). No difference was observed between IL-17$^{+/+}$ and IL-17$^{-/-}$ CD8$^+$ T cells in the cytotoxic T cell activity to H-2^d-specific P815 target cells (Figure 7C). These results indicate that IL-17 deficiency of donor T cells does not affect the development of acute GVHR.

Discussion

In the current study, we first generated IL-17$^{-/-}$ mice and demonstrated that IL-17 is involved in the development of various allergic diseases by activating allergen-

Figure 6. AHR in IL-17$^{-/-}$ Mice

(A) OVA-specific T cell proliferative response. Mesenteric LN cells from IL-17$^{+/+}$ or IL-17$^{-/-}$ mice sensitized with OVA/alum intraperitoneally were cultured in the absence or presence of 40 μg/ml OVA for 3 days. The average ± SD of triplicate experiments is shown. These results were reproducible in three independent experiments.

(B) IL-4, IL-5, and IFN-γ levels in pooled supernatant from three wells from proliferative response assay were determined by ELISA. These results were reproducible in three independent experiments.

(C) OVA-specific antibody levels after AHR. Twenty-four hours after the last challenge with OVA, sera were collected, and OVA-specific Ig levels were determined by ELISA. Each circle represents an individual mouse, and average and SD are shown.

(D) AHR to aerosolized methacholine in mice sensitized with OVA/alum intraperitoneally and challenged with OVA/PBS or PBS intranasally. Airway bronchoconstriction was assessed by enhanced respiratory pause (Penh).

(E) Total cell numbers in BALF. At 24 hr after the last inhalation of OVA/PBS or PBS in mice sensitized with OVA/alum, the trachea was cannulated and the airways were lavaged three times with 1 ml of PBS. The BALF was centrifuged, and cell numbers were counted manually.

(F) AHR in IL-17$^{-/-}$ x DO11.10 Tg mice, who were treated with OVA/PBS or PBS intranasally without prior sensation to OVA. Airway bronchoconstriction was assessed by Penh.

(G) Total cell numbers in BALF. At 24 hr after the last inhalation of OVA/PBS or PBS in IL-17$^{+/-}$ or IL-17$^{-/-}$ x DO11.10 Tg mice, BALF was collected and cell numbers were counted manually as in (E). Each circle represents an individual mouse, and average and SD are shown.

(H) Lung histology in IL-17$^{+/-}$ or IL-17$^{-/-}$ x DO11.10 Tg mice inhaled with OVA/PBS. At 24 hr after the last inhalation, the lungs were removed and sections of lung were stained with hematoxylin-eosin (×60). Symbols represent the average of each genotype mice with SD in (D) and (F). Each circle represents an individual mouse, and average and SD are shown in (C), (E), and (G). *, $p < 0.05$.

specific T cells. We have shown that the CHS response was weak in IL-17$^{-/-}$ mice, indicating involvement of IL-17 in this response.

Production of IL-17 is also reported in human skin-derived nickel-specific T cells (Albanesi et al., 2000). The CHS response is induced via multiple steps. At the initial phase, LCs in the skin migrate into LNs upon stimulation with contact allergens; then, LCs maturate in LNs and activate allergen-specific T cells through T-LC interaction in the sensitization phase; and in the elicitation phase, these allergen-primed T cells infiltrate into the skin and induce inflammation upon rechallenging with the allergens (Grabbe and Schwarz, 1998). We showed that IL-17 deficiency affected neither migration (data not shown) nor maturation of LCs (Figure 3D), although it was reported that exogenously added IL-17 promoted maturation of DCs (Antonysamy et al., 1999). Instead, we found that IL-17 is required for the activation of hapten-specific CD4$^+$ but not CD8$^+$ T cells. Adoptive transfer experiments of TNCB-immunized T cells clearly indicated that IL-17 is required for the sensitization phase.

These observations suggest that the reduced CHS response in IL-17$^{-/-}$ mice is caused by an insufficient hapten-specific CD4$^+$ T cell activation in the sensitization phase. With regard to this, it was shown previously using MHC class I$^{-/-}$ and MHC class II$^{-/-}$ mice that the effector cells in CHS response are CD8$^+$ T cells and their activity is regulated by CD4$^+$ T cells (Bouloc et al., 1998). Recently, however, it was shown using CD8$^{-/-}$ and CD4$^{-/-}$ mice that both CD8$^+$ and CD4$^+$ T cells are involved in the development of CHS, indicating that CD4$^+$ T cells are necessary for full CD8$^+$ T cell activation (Wong et al., 2000).

Proinflammatory cytokines such as IL-1 and TNF-α are known to have crucial roles in the induction of other cytokines, chemokines, and adhesion molecules that play important roles in various inflammatory responses. It has been suggested that IL-17 has activities similar to these cytokines and is also known to be a potent inducer of IL-1 and TNF-α acting on macrophages and kerationocytes (Albanesi et al., 1999, 2000; Jovanovic et al., 1998).

Although the functional discrimination and synergy among these cytokines are not completely known, there are some indications that suggest a unique role for each cytokine in the CHS reaction. In the elicitation phase, IL-1α, IL-1β, and TNF-α were produced normally at the inflammatory sites in IL-17$^{-/-}$ mice both in terms of the induction kinetics and the protein levels, indicating that the defect of the CHS reaction was directly caused by the IL-17 deficiency and not by a deficiency of other cytokines.

We showed previously that IL-1 produced by APCs is required for hapten-specific T cell activation in the sensitization phase and induces CD40L and OX40 on T cells (Nakae et al., 2001a, 2001c). At present, we do not know the molecular mechanisms for the activation of T cells by IL-17. We only know that IL-17 production by hapten-specific T cells is reduced in IL-1α/β$^{-/-}$ mice (Nakae et al., submitted). We are now analyzing the possible mechanisms.

We found that, both IL-1 and TNF-α, but not IL-17, were involved in vascular permeability at the inflammatory sites after challenge with TNCB (Figure 4B and our unpublished data). Furthermore, we showed that TNF-α was not necessary for the sensitization phase because mice that received T cells from TNF-α$^{-/-}$ mice developed a normal CHS response (Nakae et al., submitted). This finding is in clear contrast to the effect of IL-17 deficiency, in which CHS response was significantly suppressed in IL-17$^{-/-}$ T cell-transplanted mice. These observations indicate that IL-17 and TNF-α play roles in different processes. Consistent with this notion, we found that CHS response in IL-17$^{-/-}$ x TNF-α$^{-/-}$ mice was significantly lower than in single cytokine knockout mice as shown in Figure 4G.

AHR is a typical Th2-dependent immune reaction, and IL-4, IL-5, and IL-13 are believed to be the key molecules involved in the production of IgE and for the activation of mast cells and eosinophils (Lloyd et al., 2001). OVA/alum-induced AHR developed normally in IL-17$^{-/-}$ mice, although IL-4 and IL-5 production by T cells and antibody production to OVA were reduced. In contrast, AHR induced by OVA/PBS inhalation was suppressed in IL-17$^{-/-}$ x DO11.10 Tg mice. The fact that alum can induce an excess Th2 response without IL-4Rα signaling (Brewer et al., 1999) may be the cause of the difference seen between OVA/alum and OVA/PBS.

It is known that many asthmatic patients can develop dramatic pathophysiological responses to challenge with low doses of allergens (Sulakvelidze et al., 1998). This indicates that AHR model induced by OVA/PBS, rather than that by OVA/alum, seems to reflect more closely the pathology in humans. This notion is supported by the observation that B cell-deficient mice, as well as mast cell-deficient mice, exhibited a normal AHR when the animals were sensitized with OVA/alum (Korsgren et al., 1997; Takeda et al., 1997), although the generally accepted concept is that activation of mast cells by the antigen/IgE complex is crucial for the development of AHR (Martin et al., 1993). On the other hand, AHR in mast cell-deficient mice sensitized with OVA without alum was markedly suppressed (Williams and Galli, 2000). Moreover, we observed a similar phenomenon when AHR was induced with OVA in IL-1α/β$^{-/-}$ mice: AHR was suppressed only when mice were immunized with OVA/PBS but not with OVA/alum (our unpublished data). Although T cell functions such as proliferation against OVA and cytokine production were suppressed in IL-17$^{-/-}$ mice sensitized with OVA/alum, these low levels of T cell function seem to be enough to induce full AHR. These findings indicate that IL-17 is not essential for the development of allergic airway hypersensitivity under strong AHR-inducing conditions using adjuvant, but rather that IL-17 plays an important role under conditions of mild inducement through activation of allergen-specific T cells.

DTH response is a Th1 cell-mediated cellular immune response (Grabbe and Schwarz, 1998). We found that the DTH response was also impaired in IL-17$^{-/-}$ mice in the same way as in Th2-mediated AHR or Th1- and Tc1-mediated CHS, and that IL-17 was required for allergen-specific T cell activation in the sensitization phase during DTH, similarly to other responses. Thus, IL-17 seems to play an important role in activation of both Th1 and Th2 cells.

Host-versus-graft reaction (HVGR) is another T cell-

mediated immune response. Blockade of IL-17 binding with IL-17R-Fc, an IL-17R extracellular domain fused with Fc fragment, caused prolonged allograft survival (Antonysamy et al., 1999), which suggests the involvement of IL-17 in HVGR. In GVHR, however, we showed that IL-17 deficiency of donor T cells did not affect the survival of recipient B cells and that alloantigen-specific CTL activity of IL-17$^{-/-}$ CD8$^+$ T cells was normal. These observations indicate that donor CD4$^+$ T cell-produced IL-17 is not required for allo-specific CD8$^+$ T cell activation in acute GVHR. Consistent with this, it was reported that expansion of allo-specific CD8$^+$ T cells occurred in acute GVHR without the help of CD4$^+$ T cells, the major producer of IL-17 (Buhlmann et al., 1999).

We showed that antigen-specific antibody production was significantly decreased in IL-17$^{-/-}$ mice. This effect of IL-17 deficiency was not affected by the route of immunization or the presence of adjuvant. The suppression of antibody production was observed in the CHS response, in which mice were sensitized with allergens via the skin route without adjuvants; in the DTH response, in which mice were immunized intraperitoneally with CFA; and in AHR, in which immunization was carried out intraperitoneally with alum. Since IL-17 deficiency did not have any direct effects on B cells as assessed by the response against mitogenic stimuli such as LPS, anti-IgM mAb, and anti-CD40 mAb (data not shown), these findings suggest that the observed defects on antibody production are due to insufficient B cell activation by IL-17$^{-/-}$ T cells.

Taken together, this study shows that IL-17 plays a crucial role in allergen-specific cellular and humoral immune responses through the activation of T cells, and we have also provided insights into molecular mechanisms for the development of CHS, DTH and AHR. It should be noted that IL-17 is specific because it mediates both Th1-dominant allergic reactions such as CHS, DTH, and collagen-induced arthritis (our unpublished data), and Th2-dominant reactions such as AHR. It is reported that IL-17 is produced by a specific T cell subpopulation that does not belong to Th1 or Th2 subpopulations and produces TNF-α and/or GM-CSF simultaneously (Infante-Duarte et al., 2000). Thus, these observations indicate that IL-17 belongs to a distinct category of cytokine that belongs to neither Th1 nor Th2 cytokines. These findings should be useful for the development of therapeutics for these diseases. Using these IL-17$^{-/-}$ mice, we are now examining the possibility that IL-17 is also involved in the development of other T cell-mediated autoimmune diseases such as collagen-induced arthritis, inflammatory bowel disease, and experimental autoimmune encephalomyelitis.

Experimental Procedures

Generation of IL-17$^{-/-}$ Mice

Genomic DNA containing the *il-17* gene was isolated from mouse 129/SVJ genomic phage library (Stratagene, La Jolla, CA). A targeting vector was constructed by replacing 2.1 kb genomic fragment with the 2.5 kb DNA fragment containing the *EGFP* gene and *neomycin resistance* gene (*neo*) under the control of the phosphoglycerate kinase (PGK) 1 promoter which was flanked by lox P sequences. The fragment contained the first and second exons, which ranged from the initiation codon ATG to a SnaBI site between the second and third exons. A *diphtheria toxin A* (*DT*) gene under the MC1 promoter was ligated to the 5′ end of the targeting vector for negative selection. The targeting vector was electroporated into ES (E14.1) cells and selected in G418 (Asano et al., 1997). Targeted clones were screened by Southern blot hybridization analysis using 5′ and 3′ probes. Two clones out of seven independently identified targeted ES clones were treated with Adeno virus carrying the *cre* gene to delete the *neo* gene (Kanegae et al., 1995). Chimera mice were generated by the aggregation method using C57BL/6J blastocysts as the recipients (Asano et al., 1997). Chimera mice were mated with C57BL/6J female mice for germline transmission. For AHR, IL-17$^{-/-}$ mice were backcrossed to BALB/cA mice for three generations, and then crossed to DO11.10 transgenic mice, which were kindly provided by Dr. Dennis Y. Loh (Washington University School of Medicine). For CHS and DTH, littermates of IL-17$^{-/-}$ mice on 129 x B6 F1 background were used. The genotyping of IL-17$^{-/-}$ mice was carried out using the following PCR primers: primer 1, 5′-ACTCTTCATCCACCTCACACGA-3′; primer 2, 5′-GCCATGATATA GACGTTGTGGC-3′; primer 3, 5′-CAGCATCAGAGACTAGAAGGGA-3′. Primers 1 and 2 were used to detect wild-type allele (1.3 kb), and primers 1 and 3 were used to detect mutant allele (0.5 kb). TNF-α$^{-/-}$ mice were backcrossed to C57BL/6J mice for ten generations and used for the experiments.

All the mice were kept under specific pathogen-free conditions in an environmentally controlled clean room in the Laboratory Animal Research Center, Institute of Medical Science, University of Tokyo. The experiments were conducted according to the institutional ethical guidelines for animal experiments and the safety guidelines for gene manipulation experiments.

Cell Proliferation Assay

Cell preparation and mitogenic response were performed as described previously (Nakae et al., 2001a, 2001b). To measure the mBSA- or OVA-specific LN cell response, LN cells (4×10^5 cells/well) were cultured in the absence or presence of 40 μg/ml of mBSA or OVA for 3 days, respectively, followed by incorporation of [^{3}H] thymidine (0.25 μCi/ml) (Amersham, Buckinghamshire, England) for 6 hr. Data shown are from the time point of the maximal response.

ELISA for Cytokines and Antigen-Specific Igs

For cytokine ELISA, monoclonal rat anti-mouse IL-17 (DAKO, Carpinteria, CA), hamster anti-mouse IL-1α mAb (Genzyme, Cambridge, MA), hamster anti-mouse IL-1β mAb (Genzyme), and anti-mouse TNF-α mAb (ENDOGEN, Woburn, MA) as capture Abs and polyclonal biotinylated goat anti-mouse IL-17 antibody (DAKO), rabbit anti-mouse IL-1α (Genzyme), rabbit anti-mouse IL-1β (Genzyme), and rabbit anti-mouse TNF-α (provided by Dr. Katsuo Noguchi, Teikyo University) as the second antibodies were used. HRP-avidin and HRP-conjugated goat anti-rabbit IgG was purchased from PharMingen and Zymed (San Francisco, CA), respectively. TMB substrate was purchased from DAKO. ELISA for IL-4, IL-5, and IFN-γ was performed as previously described (Nakae et al., 2001b). TNP-, mBSA-, and OVA-specific Ig levels were measured by ELISA as previously described (Nakae et al., 2001a, 2001c; Ohshima et al., 1998).

CHS

TNCB-induced CHS, TNP-specific T cell proliferation, LC preparation and maturation, and intracellular staining of FITC$^+$CD11c$^+$ LCs were assayed as described previously (Nakae et al., 2001c). In brief, abdomen of mice were sensitized epicutaneously with TNCB; then, 5 days later, the ear was challenged with 1% TNCB. At 24 hr after the second challenge, mice were euthanized, and discs of ear tissue were removed and weighed. Ear swelling was calculated as follows; (Increment of ear swelling [mg]) = {(weight of challenged ear [mg]) − (weight of vehicle-treated ear [mg])}. For FACS staining, PE-anti-mouse CD40 mAb (3.23; Immunotech, Marseille Cedex, France), PE-anti-mouse CD86 mAb (RMMP-1; Immunotech), and PE anti-IL-12 p40/p70 (C15.6: kindly provided by Dr. T. Tamura) were used. For DC transfer, TNP-conjugated CD11c$^+$ splenic DCs (5×10^5 cells) were transferred into nontreated mice, and then DC-transferred mice were challenged with TNCB. DNFB-induced CHS, DNP-specific T cell response, and adoptive T cell transfer were performed according to Chen et al. (1999). For reconstitution assay, CD4$^+$ T

cells (4×10^7 cells) from IL-17$^{+/+}$ mice were injected into nontreated IL-17$^{+/+}$ or IL-17$^{-/-}$ mice, and the next day, these mice were sensitized and challenged with TNCB. Vascular permeability was examined with a modification of the method described previously (Rauschmayr et al., 1997). At 5 min after the challenge with 1.0% TNCB, 8.3 μl/g body weight of 1.0% Evans blue dye (WAKO, Osaka, Japan) in PBS was injected through the tail vein. One hour later, a 6 mm diameter biopsy was taken from a TNCB- and/or vehicle-treated ear, Evans blue dye in the tissues was extracted in acetone, and the absorbancy at 650 nm was measured. A 6 mm diameter biopsy was taken from the TNCB- or vehicle-challenged ear, and after homogenization, MPO activity was measured as previously described (Higgins et al., 1999).

DTH

mBSA-induced DTH was examined as previously described (Zheng et al., 1995). In brief, mice were sensitized with 1.25 mg/ml mBSA (SIGMA, St. Louis, MO) with complete Freund's adjuvant (CFA; Difco, Detroit, MI) subcutaneously at the base of the tail. Seven days after sensitization, mice were challenged with 200 μg/20 μl mBSA into one footpad, and an equal volume of PBS was injected into another footpad. The footpad swelling was measured by a dial caliper and calculated as follows: (footpad swelling [%]) = {(footpad thickness of mBSA-injected footpad [mm]) − (footpad thickness of PBS-injected footpad [mm])} + (footpad thickness of PBS-injected footpad [mm]) × 100.

AHR

Mice were sensitized with 100 μg/ml OVA/alum intraperitoneally on days 0 and 12, and 21 days later mice were challenged with 100 ng of OVA/PBS intranasally once a day for 3 days. For OVA/PBS-induced AHR, IL-17$^{+/-}$ or IL-17$^{-/-}$ mice crossed with DO11.10 Tg mice were made to inhale 100 ng of OVA/PBS intranasally every day for 4 days. Twenty-four hours after the last inhalation, AHR to methacholine was assessed using the parameter Penh (enhanced pause), which is calculated automatically based on the mean pressure generated in plethysmograph chambers during inspiration and expiration with the Buxco system as described elsewhere (Williams and Galli, 2000).

Acute GVHR

Acute GVHR was examined as previously described (Buhlmann et al., 1999). Splenocytes (6×10^7 cells) of IL-17$^{+/+}$ or IL-17$^{-/-}$ mice backcrossed to C57BL/6J mice for four generations were injected into a (C57BL/6 × BALB/c)F1 (CBF1) mouse intravenously. Anti-mouse CD16/CD32 (2.4G2), PE anti-mouse CD4 (RM4-5), PE anti-mouse CD8 (53-6.72), PE anti-mouse CD45R/B220 (RA3-6B2), and FITC anti-mouse H-2K^d (SF1-1.1) for FACS analysis were obtained from PharMingen. Spleen cell proliferation was examined 10 days after the transfer. After incubation with biotinylated anti-mouse H-2K^d and streptavidin-beads, H-2K^d−CD8$^+$ T cells were purified using MACS columns and used as the effector cells for CTL assay. P815 cells were used as target cells, and ^{51}Cr release was measured according to a standard protocol.

Statistics

Student's t test was used for statistical evaluation of the results.

Acknowledgments

We thank Ms. Kazumi Ebine and Ms. Tomoko Hata for their technical support in the experiments and all the members of the laboratory for excellent animal care. We also thank Dr. Toshiki Tamura (Institute of Medical Science, University of Tokyo) for anti-IL-12 mAb. This work was supported by grants from the Ministry of Education, Science, Sport and Culture of Japan and the Ministry of Health and Welfare of Japan.

Received: March 13, 2002
Revised: August 9, 2002

References

Aarvak, T., Chabaud, M., Miossec, P., and Natvig, J.B. (1999). IL-17 is produced by some proinflammatory Th1/Th0 cells but not by Th2 cells. J. Immunol. *162*, 1246–1251.

Aggarwal, S., and Gurney, A.L. (2002). IL-17: prototype member of an emerging cytokine family. J. Leukoc. Biol. *71*, 1–8.

Albanesi, C., Cavani, A., and Girolomoni, G. (1999). IL-17 is produced by nickel-specific T lymphocytes and regulates ICAM-1 expression and chemokine production in human keratinocytes: synergistic or antagonist effects with IFN-gamma and TNF-alpha. J. Immunol. *162*, 494–502.

Albanesi, C., Scarponi, C., Cavani, A., Federici, M., Nasorri, F., and Girolomoni, G. (2000). Interleukin-17 is produced by both Th1 and Th2 lymphocytes, and modulates interferon-gamma- and interleukin-4-induced activation of human keratinocytes. J. Invest. Dermatol. *115*, 81–87.

Antonysamy, M.A., Fanslow, W.C., Fu, F., Li, W., Qian, S., Troutt, A.B., and Thomson, A.W. (1999). Evidence for a role of IL-17 in organ allograft rejection: IL-17 promotes the functional differentiation of dendritic cell progenitors. J. Immunol. *162*, 577–584.

Asano, M., Furukawa, K., Kido, M., Matsumoto, S., Umesaki, Y., Kochibe, N., and Iwakura, Y. (1997). Growth retardation and early death of beta-1,4-galactosyltransferase knockout mice with augmented proliferation and abnormal differentiation of epithelial cells. EMBO J. *16*, 1850–1857.

Attur, M.G., Patel, R.N., Abramson, S.B., and Amin, A.R. (1997). Interleukin-17 up-regulation of nitric oxide production in human osteoarthritis cartilage. Arthritis Rheum. *40*, 1050–1053.

Bouloc, A., Cavani, A., and Katz, S.I. (1998). Contact hypersensitivity in MHC class II-deficient mice depends on CD8 T lymphocytes primed by immunostimulating Langerhans cells. J. Invest. Dermatol. *111*, 44–49.

Brewer, J.M., Conacher, M., Hunter, C.A., Mohrs, M., Brombacher, F., and Alexander, J. (1999). Aluminium hydroxide adjuvant initiates strong antigen-specific Th2 responses in the absence of IL-4- or IL-13-mediated signaling. J. Immunol. *163*, 6448–6454.

Buhlmann, J.E., Gonzalez, M., Ginther, B., Panoskaltsis-Mortari, A., Blazar, B.R., Greiner, D.L., Rossini, A.A., Flavell, R., and Noelle, R.J. (1999). Cutting edge: sustained expansion of CD8+ T cells requires CD154 expression by Th cells in acute graft versus host disease. J. Immunol. *162*, 4373–4376.

Chen, A.I., McAdam, A.J., Buhlmann, J.E., Scott, S., Lupher, M.L., Jr., Greenfield, E.A., Baum, P.R., Fanslow, W.C., Calderhead, D.M., Freeman, G.J., and Sharpe, A.H. (1999). Ox40-ligand has a critical costimulatory role in dendritic cell:T cell interactions. Immunity *11*, 689–698.

Fossiez, F., Banchereau, J., Murray, R., Van Kooten, C., Garrone, P., and Lebecque, S. (1998). Interleukin-17. Int. Rev. Immunol. *16*, 541–551.

Grabbe, S., and Schwarz, T. (1998). Immunoregulatory mechanisms involved in elicitation of allergic contact hypersensitivity. Immunol. Today *19*, 37–44.

Higgins, L.M., McDonald, S.A., Whittle, N., Crockett, N., Shields, J.G., and MacDonald, T.T. (1999). Regulation of T cell activation in vitro and in vivo by targeting the OX40-OX40 ligand interaction: amelioration of ongoing inflammatory bowel disease with an OX40-IgG fusion protein, but not with an OX40 ligand-IgG fusion protein. J. Immunol. *162*, 486–493.

Hirahara, N., Nio, Y., Sasaki, S., Takamura, M., Iguchi, C., Dong, M., Yamasawa, K., Itakura, M., and Tamura, K. (2000). Reduced invasiveness and metastasis of Chinese hamster ovary cells transfected with human interleukin-17 gene. Anticancer Res. *20*, 3137–3142.

Infante-Duarte, C., Horton, H.F., Byrne, M.C., and Kamradt, T. (2000). Microbial lipopeptides induce the production of IL-17 in Th cells. J. Immunol. *165*, 6107–6115.

Jovanovic, D.V., Di Battista, J.A., Martel-Pelletier, J., Jolicoeur, F.C., He, Y., Zhang, M., Mineau, F., and Pelletier, J.P. (1998). IL-17 stimulates the production and expression of proinflammatory cytokines,

IL-beta and TNF-alpha, by human macrophages. J. Immunol. *160*, 3513–3521.

Kanegae, Y., Lee, G., Sato, Y., Tanaka, M., Nakai, M., Sakaki, T., Sugano, S., and Saito, I. (1995). Efficient gene activation in mammalian cells by using recombinant adenovirus expressing site-specific Cre recombinase. Nucleic Acids Res. *23*, 3816–3821.

Korsgren, M., Erjefalt, J.S., Korsgren, O., Sundler, F., and Persson, C.G. (1997). Allergic eosinophil-rich inflammation develops in lungs and airways of B cell-deficient mice. J. Exp. Med. *185*, 885–892.

Kotake, S., Udagawa, N., Takahashi, N., Matsuzaki, K., Itoh, K., Ishiyama, S., Saito, S., Inoue, K., Kamatani, N., Gillespie, M.T., et al. (1999). IL-17 in synovial fluids from patients with rheumatoid arthritis is a potent stimulator of osteoclastogenesis. J. Clin. Invest. *103*, 1345–1352.

Lloyd, C.M., Gonzalo, J.A., Coyle, A.J., and Gutierrez-Ramos, J.C. (2001). Mouse models of allergic airway disease. Adv. Immunol. *77*, 263–295.

Martin, T.R., Takeishi, T., Katz, H.R., Austen, K.F., Drazen, J.M., and Galli, S.J. (1993). Mast cell activation enhances airway responsiveness to methacholine in the mouse. J. Clin. Invest. *91*, 1176–1182.

Matusevicius, D., Kivisakk, P., He, B., Kostulas, N., Ozenci, V., Fredrikson, S., and Link, H. (1999). Interleukin-17 mRNA expression in blood and CSF mononuclear cells is augmented in multiple sclerosis. Mult. Scler. *5*, 101–104.

Nakae, S., Asano, M., Horai, R., Sakaguchi, N., and Iwakura, Y. (2001a). IL-1 enhances T cell-dependent antibody production through induction of CD40 ligand and OX40 on T cells. J. Immunol. *167*, 90–97.

Nakae, S., Horai, R., Asano, M., and Iwakura, I. (2001b). Interleukin-1β, but not Interleukin-1α, is required for T-cell-dependent antibody production. Immunology *104*, 402–409.

Nakae, S., Naruse-Nakajima, C., Sudo, K., Horai, R., Asano, M., and Iwakura, Y. (2001c). IL-1α, but not IL-1β, is required for contact-allergen-specific T cell activation during the sensitization phase in contact hypersensitivity. Int. Immunol. *13*, 1471–1478.

Ohshima, S., Saeki, Y., Mima, T., Sasai, M., Nishioka, K., Nomura, S., Kopf, M., Katada, Y., Tanaka, T., Suemura, M., and Kishimoto, T. (1998). Interleukin 6 plays a key role in the development of antigen-induced arthritis. Proc. Natl. Acad. Sci. USA *95*, 8222–8226.

Rauschmayr, T., Groves, R.W., and Kupper, T.S. (1997). Keratinocyte expression of the type 2 interleukin 1 receptor mediates local and specific inhibition of interleukin 1-mediated inflammation. Proc. Natl. Acad. Sci. USA *94*, 5814–5819.

Rouvier, E., Luciani, M.F., Mattei, M.G., Denizot, F., and Golstein, P. (1993). CTLA-8, cloned from an activated T cell, bearing AU-rich messenger RNA instability sequences, and homologous to a herpesvirus saimiri gene. J. Immunol. *150*, 5445–5456.

Schwandner, R., Yamaguchi, K., and Cao, Z. (2000). Requirement of tumor necrosis factor receptor-associated factor (TRAF)6 in interleukin 17 signal transduction. J. Exp. Med. *191*, 1233–1240.

Schwarzenberger, P., Huang, W., Ye, P., Oliver, P., Manuel, M., Zhang, Z., Bagby, G., Nelson, S., and Kolls, J.K. (2000). Requirement of endogenous stem cell factor and granulocyte-colony-stimulating factor for IL-17-mediated granulopoiesis. J. Immunol. *164*, 4783–4789.

Shalom-Barak, T., Quach, J., and Lotz, M. (1998). Interleukin-17-induced gene expression in articular chondrocytes is associated with activation of mitogen-activated protein kinases and NF-kappaB. J. Biol. Chem. *273*, 27467–27473.

Shin, H.C., Benbernou, N., Esnault, S., and Guenounou, M. (1999). Expression of IL-17 in human memory CD45RO+ T lymphocytes and its regulation by protein kinase A pathway. Cytokine *11*, 257–266.

Sulakvelidze, I., Inman, M.D., Rerecich, T., and O'Byrne, P.M. (1998). Increases in airway eosinophils and interleukin-5 with minimal bronchoconstriction during repeated low-dose allergen challenge in atopic asthmatics. Eur. Respir. J. *11*, 821–827.

Takeda, K., Hamelmann, E., Joetham, A., Shultz, L.D., Larsen, G.L., Irvin, C.G., and Gelfand, E.W. (1997). Development of eosinophilic airway inflammation and airway hyperresponsiveness in mast cell-deficient mice. J. Exp. Med. *186*, 449–454.

Williams, C.M., and Galli, S.J. (2000). Mast cells can amplify airway reactivity and features of chronic inflammation in an asthma model in mice. J. Exp. Med. *192*, 455–462.

Wong, C.K., Ho, C.Y., Li, E.K., and Lam, C.W. (2000). Elevation of proinflammatory cytokine (IL-18, IL-17, IL-12) and Th2 cytokine (IL-4) concentrations in patients with systemic lupus erythematosus. Lupus *9*, 589–593.

Wong, C.K., Ho, C.Y., Ko, F.W., Chan, C.H., Ho, A.S., Hui, D.S., and Lam, C.W. (2001). Proinflammatory cytokines (IL-17, IL-6, IL-18 and IL-12) and Th cytokines (IFN-gamma, IL-4, IL-10 and IL-13) in patients with allergic asthma. Clin. Exp. Immunol. *125*, 177–183.

Yao, Z., Fanslow, W.C., Seldin, M.F., Rousseau, A.M., Painter, S.L., Comeau, M.R., Cohen, J.I., and Spriggs, M.K. (1995a). Herpesvirus Saimiri encodes a new cytokine, IL-17, which binds to a novel cytokine receptor. Immunity *3*, 811–821.

Yao, Z., Painter, S.L., Fanslow, W.C., Ulrich, D., Macduff, B.M., Spriggs, M.K., and Armitage, R.J. (1995b). Human IL-17: a novel cytokine derived from T cells. J. Immunol. *155*, 5483–5486.

Ye, P., Rodriguez, F.H., Kanaly, S., Stocking, K.L., Schurr, J., Schwarzenberger, P., Oliver, P., Huang, W., Zhang, P., Zhang, J., et al. (2001). Requirement of interleukin 17 receptor signaling for lung CXC chemokine and granulocyte colony-stimulating factor expression, neutrophil recruitment, and host defense. J. Exp. Med. *194*, 519–527.

Zheng, H., Fletcher, D., Kozak, W., Jiang, M., Hofmann, K.J., Conn, C.A., Soszynski, D., Grabiec, C., Trumbauer, M.E., Shaw, A., et al. (1995). Resistance to fever induction and impaired acute-phase response in interleukin-1 β-deficient mice. Immunity *3*, 9–19.

Cell Death and Differentiation (2002) 9, 1196–1206

www.nature.com/cdd

Ex vivo whole-embryo culture of caspase-8-deficient embryos normalize their aberrant phenotypes in the developing neural tube and heart

K Sakamaki*[,1], T Inoue[2], M Asano[3,7], K Sudo[3], H Kazama[1], J Sakagami[3], S Sakata[1], M Ozaki[4], S Nakamura[2], S Toyokuni[5], N Osumi[6], Y Iwakura[3] and S Yonehara*[,1]

[1] Graduate School of Biostudies and Institute for Virus Research, Kyoto University, Sakyo-ku, Kyoto 606-8507, Japan
[2] Division of Biochemistry and Cell Biology, National Institute of Neuroscience, National Center of Neurology and Psychiatry, Kodaira 187-8502, Japan
[3] Center for Experimental Medicine, Institute of Medical Science, University of Tokyo, Minato-ku, Tokyo 108-8639, Japan
[4] Laboratory for Neural Architecture, Brain Science Institute, The Institute of Physical and Chemical Research, RIKEN, Wako 351-0198, Japan
[5] Department of Pathology and Biology of Diseases, Graduate School of Medicine, Kyoto University, Sakyo-ku, Kyoto 606-8501, Japan
[6] Department of Developmental Neurobiology, Graduate School of Medicine, Tohoku University, Aoba-ku, Sendai 980-8575, Japan
[7] Present address: Institute for Experimental Animals, Graduate School of Medicine, Kanazawa University, Kanazawa 920-8640, Japan
* Corresponding authors: K Sakamaki, Shogoin-Kawaramachi 53, Sakyo-ku, Kyoto 606-8507, Japan. Tel.: 81-75-751-4786; Fax: 81-75-751-4784; E-mail: ksakamak@virus.kyoto-u.ac.jp and S Yonehara, Shogoin-Kawaramachi 53, Sakyo-ku, Kyoto 606-8507, Japan. Tel.: 81-75-751-4783; Fax: 81-75-751-4784; E-mail: syonehar@virus.kyoto-u.ac.jp

Received 20.3.02; revised 6.4.02; accepted 7.6.02
Edited by H Ichijo

Abstract

Caspase-8 plays the role of initiator in the caspase cascade and is a key molecule in death receptor-induced apoptotic pathways. To investigate the physiological roles of caspase-8 *in vivo*, we have generated caspase-8-deficient mice by gene targeting. The first signs of abnormality in homozygous mutant embryos were observed in extraembryonic tissue, the yolk sac. By embryonic day (E) 10.5, the yolk sac vasculature had begun to form inappropriately, and subsequently the mutant embryos displayed a variety of defects in the developing heart and neural tube. As a result, all mutant embryos died at E11.5. Importantly, homozygous mutant neural and heart defects were rescued by *ex vivo* whole-embryo culture during E10.5–E11.5, suggesting that these defects are most likely secondary to a lack of physiological caspase-8 activity. Taken together, these results suggest that caspase-8 is indispensable for embryonic development.
Cell Death and Differentiation (2002) 9, 1196–1206. doi:10.1038/sj.cdd.4401090

Keywords: caspase-8; apoptosis; hemorrhage; cardiac rupture; angiogenesis; whole-embryo culture

Abbreviations: ES, embryonic stem; FADD, Fas-associated death domain protein; MEF, mouse embryonic fibroblasts; PBS, phosphate-buffered saline; PECAM-1, platelet endothelial cell adhesion molecule-1; PFA, paraformaldehyde; RT–PCR, reverse-transcriptase and polymerase chain reaction; TUNEL, terminal deoxynucleotidyl transferase-mediated dUTP-digoxigenin nick-end labeling

Introduction

Apoptosis, or programmed cell death, is the principal mechanism utilized by multicellular organisms to orchestrate tissue morphogenesis during development and maintain homeostasis in adulthood.[1–3] Apoptosis also occurs during defense processes and immune responses.[4] Studies on signal transduction mechanisms in apoptosis identified several molecules which effect and regulate this process. Of these molecules, caspases, a family of cysteine proteases, have been shown to act as the executioners of apoptosis.[5] In mammals, fourteen caspases have been identified, most of which are activated during apoptosis. Among these, caspase-8 (also known as FLICE/MACH/Mch5) is an initiator caspase with a long prodomain, termed a 'death effector domain' (DED), which activates downstream effector caspases (e.g. caspase-3, -6 and -7).[6,7] It has been shown that caspase-8 is essential for Fas-mediated apoptotic signaling.[8,9] Ligation of Fas results in the recruitment of caspase-8 via interaction with the adapter molecule FADD (Fas-associated death domain protein, also called MORT1). Recruitment of caspase-8 to the complex initiates autoprocessing of procaspase-8 to an active form which is released into the cytoplasm.[10] Activated caspase-8 cleaves and activates downstream caspases, thereby committing the cell to apoptosis. Caspase-8 also activates another apoptotic pathway, which, through processing of Bid, mediates release of cytochrome *c* from mitochondria and activation of caspase-9.[11] And, in addition to Fas, caspase-8 is involved in apoptotic signaling via other death receptors, such as tumor necrosis factor receptor type 1 (TNFR1), death receptor 3 (DR3) and TNF-related apoptosis-inducing ligand (TRAIL) receptors.[12–15] Clearly, caspase-8 is an important mediator for a wide range of apoptotic pathways.

During embryogenesis, apoptosis is utilized ubiquitously to eliminate unwanted or excess cells in the organism. Recently, the targeted disruption of several genes involved in apoptosis has been performed.[16,17] Among those analyzed, it has been shown that caspase-3, caspase-9 and Apaf-1 are involved in brain development during late embryogenesis.[18–22] Targeted disruption of mouse FADD results in developmental heart abnormalities and embryonic lethality.[23,24] Furthermore, caspase-8-deficient mice display impaired heart muscle development and accumulation of

erythrocytes in the liver.[12] More recently, it has been reported that Casper (also called c-FLIP), which negatively regulates Fas-mediated apoptosis by interacting with FADD or/and caspase-8, is also involved in heart development during embryogenesis.[25] Taken together, evidence from FADD-, Casper- and caspase-8-deficient mice suggests that these molecules function in a Fas-independent manner during embryogenesis.

To investigate the biological function of caspase-8 *in vivo*, we generated mutant mice devoid of proteolytic function by targeted disruption of the protease domain using homologous recombination. Like the previous report on this knockout model,[12] we found that protease-deficient caspase-8 mutants die *in utero* and exhibit cardiac rupture. Moreover, we report the new finding of several additional embryonic and extraembryonic defects which arise during embryogenesis. We also report that our caspase-8 mutant embryos could be rescued by *ex vivo* whole-embryo culture, a finding which could help point to an explanation of the defects displayed by our mice. The present study suggests first the direct involvement of caspase-8 in early mouse embryonic development, particularly in organogenesis.

Results

Embryonic expression of caspase-8

In a previous study, we demonstrated that caspase-8 is expressed in adult tissues as well as in embryos at 9.5 days (E9.5) and 17 days (E17) of development by Northern blot analysis.[28] To confirm these findings, we further analyzed caspase-8 expression in embryos at the protein level (Figure 1). We prepared cell lysates from E8.5 embryos and from various tissues of E17 embryos and analyzed them by immunoblotting with an anti-mouse caspase-8 monoclonal antibody. As a positive control, we used cell lysates from JB-6 stable transfectants expressing mouse caspase-8. We detected a 55-kDa protein in JB-6 transfectants, but not in parental JB-6 cells lacking endogenous caspase-8 (Figure 1, lanes 14 and 15). Similarly, we observed a strong band of the same size in E8.5 embryos and in the thymus, skin and muscle of E17 embryos (Figure 1, lanes 1, 2, 9 and 10). A faint band was observed in cell lysates from the spleen, kidney, stomach, heart, intestine and lung (lanes 3–8). Caspase-8 could not be detected in the liver and brain (Figure 1, lanes 11–13). Taken together, these data strongly suggest that caspase-8 is expressed in several tissues during mouse embryogenesis, at least between E8.5 and E17. To help determine the role played by caspase-8 during this period, we created caspase-8 knockout mice by targeted disruption.

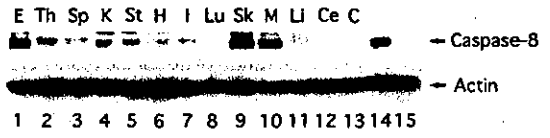

Figure 1 Immunoblot analysis of caspase-8 in mouse embryos. Approximately 70 μg of cell lysates from E8.5 embryos (lane 1) and from various E17 embryonic tissues (lanes 2–13) were analyzed by SDS–PAGE followed by immunoblotting with anti-mouse caspase-8 antibody. Cell lysates from JB-6 transfectants expressing mouse caspase-8 and from parental JB-6 cells were also analyzed (lanes 14 and 15). Blots were also probed with anti-actin antibody as a standard control. Abbreviations: E, E8.5 embryo; Th, thymus; Sp, spleen; K, kidney; St, stomach; H, heart; I, intestine; Lu, lung; Sk, skin; M, muscle; Li, liver; Ce, cerebrum; C, cerebellum

Targeted disruption of the mouse caspase-8 gene and generation of caspase-8 knockout mice

Caspase-10 (also known as FLICE2/Mch4), a caspase-8 homologue, plays a similar role to caspase-8 in Fas-mediated apoptotic signaling in humans,[27] and it was thought that caspase-10 might compensate for the lack of caspase-8 activity in caspase-8-null mice. We speculated that a truncated caspase-8 protein lacking the protease domain might act as a dominant-negative molecule and inhibit the function of caspase-10. To generate this caspase-8 mutant, we designed a targeting vector by which a stop codon and SV40 polyadenylation sequence would be inserted into exon 7 of the caspase-8 gene (Figure 2A). After transfection of the targeting vector and selection with G418, four homologous recombinant embryonic stem (ES) clones were isolated (Figure 2B), two of which were used to produce chimeric mice. Finally, we established independent lines of caspase-8 knockout mice from six chimerae and examined their progenies.

Embryonic lethality of homozygous caspase-8-deficient mice

The established heterozygous mutants displayed normal phenotype and retained propagative activity. However, no homozygous mutants were observed among live pups genotyped from heterozygous mating, indicating that homozygous mutants are embryonic lethal. Therefore, we examined embryos of various stages (Table 1), and found that until E10.5, homozygous mutant embryos were detected in the expected Mendelian ratio (25%). However, all homozygous mutants obtained at later timepoints (E11.5 to E14.5) died accompanying with abnormal phenotypes. Most homozygous mutant embryos displayed signs of abdominal hemorrhage (described below in detail). This phenotype, observed in all of our mutant lines, was similar to that of caspase-8 null-mutant mice.[12] However, by reverse-transcriptase and polymerase chain reaction (RT–PCR) analysis of embryonic transcripts, we were able to detect truncated caspase-8 mRNA transcribed from the mutant allele (Figure 2C). Furthermore, by immunoblot analysis with an anti-caspase-8 antibody, a 55-kDa pro-caspase-8 was detected in wild-type mouse embryonic fibroblasts (MEFs), but not in homozygous mutant MEFs, whereas a peptide at 25 kDa corresponding to the DED domains of caspase-8 was observed in mutant MEFs (Figure 2D). These results suggest that our mice exhibit protease-deficient mutation, but not null-mutation, of the caspase-8 gene. We designate our homozygous mutant mice as *caspase-8*$^{DED/DED}$.

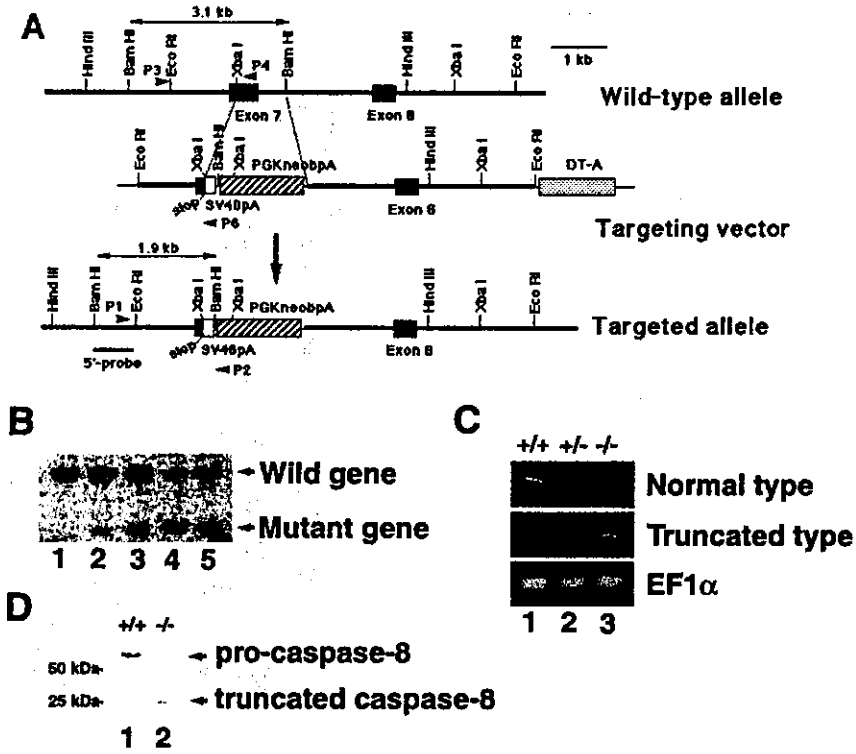

Figure 2 Targeted disruption of the mouse caspase-8 gene by homologous recombination. (A) Targeting strategy for homologous recombination. Exons of the caspase-8 gene are depicted as closed boxes. The SV40 polyA sequence, the PGKneobpA cassette and the diphtheria toxin A fragment gene (DT-A) cassette are indicated by open, hatched and dotted boxes, respectively. Primers (P1, P2, P3, P4 and P6) used for screening and RT–PCR are shown by arrowheads. A 5'-probe for Southern hybridization and DNA fragments expected after *Bam*HI digestion are indicated by a bold line and arrows, respectively. (B) Southern blot analysis of ES cell clones. Genomic DNAs isolated from parental cells (lane 1) and ES clones (lanes 2–5) were digested with *Bam*HI, resolved by electrophoresis and hybridized with a 5'-probe. The 3.1 kb and 1.9 kb DNA bands correspond to the wild-type and mutant genes, respectively. (C) RT–PCR analysis of caspase-8-deficient embryos. Total RNAs from E10.5 embryos obtained by crossing heterozygotic mice were amplified as described in Materials and Methods. PCR products derived from wild-type embryo (lane 1) and heterozygous (lane 2) and homozygous (lane 3) mutant embryos were analyzed by electrophoresis for detection of normal (top) and truncated (middle) caspase-8 transcripts. Primers for mouse EF1α transcripts were used as a standard control (bottom). (D) Immunoblot analysis of MEFs. Cell lysates of wild-type (+/+) and homozygous caspase-8 mutant (−/−) MEF cells were analyzed by SDS–PAGE followed by immunoblotting with anti-mouse caspase-8 monoclonal antibody specific to the DED domain of caspase-8. Size standards are shown on the left side

Table 1 Genotyping of mice derived from caspase-8 heterozygous intercrosses

Age (days)	No. of genotypes (%) +/+	+/−	−/−	No. of abnormal −/− homozygotes* (%)
P21-28	22 (30)	51 (70)	0 (0)	
E14.5-	48 (36)	71 (53)	15 (11)	15/15 (100)
E12.5	18 (32)	31 (58)	6 (10)	6/6 (100)
E11.5	48 (27)	100 (60)	24 (13)	24/24 (100)
E10.5	72 (33)	87 (42)	54 (25)	3/54 (6)
E9.5	16 (34)	21 (46)	9 (20)	0/9 (0)
E8.5	6 (37)	8 (50)	2 (13)	0/2 (0)

The genotype of mice at indicated postnatal (P) or embryonic (E) days were determined by PCR analysis. *Morphology of the homozygous mutants were judged under the microscope.

Extraembryonic defects in *caspase-8*$^{DED/DED}$ mutant embryos

Abnormal development of *caspase-8*$^{DED/DED}$ mutant mice was first observed in the extraembryonic tissue, the yolk sac. The yolk sac of the E11.5 *caspase-8*$^{DED/DED}$ mouse appears pale and displays underdeveloped vasculature (Figure 3A). To analyze these defects, we examined the yolk sac vascular endothelium using an antibody specific for platelet endothelial cell adhesion molecule-1 (PECAM-1/CD31) (Figure 3B). In wild-type yolk sacs, the vascular network was pruned and remodeled to form a branched and intricate tree-like network between E9.5 and E11.5. In contrast, *caspase-8*$^{DED/DED}$ yolk sacs still exhibited the honeycomb-like primary capillary plexus at E10.5. Eventually, regression of vessels was observed in the E11.5 mutant yolk sac. Upon histological

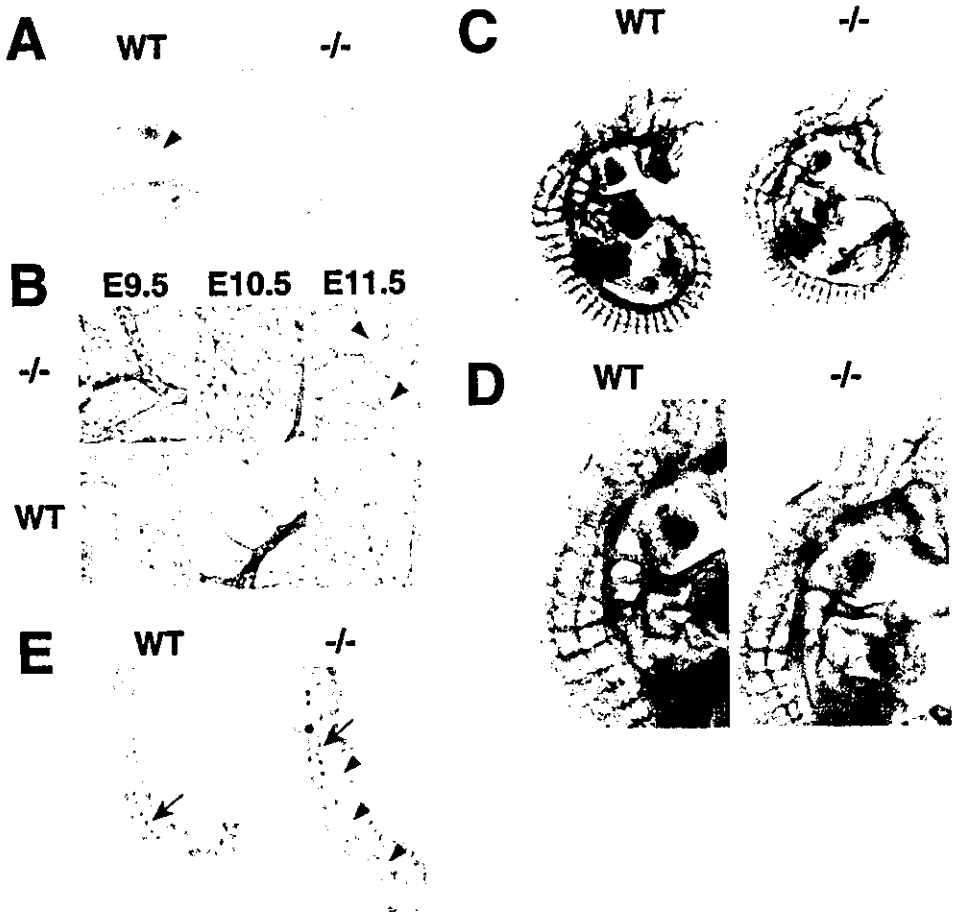

Figure 3 Yolk sac defects in caspase-8-deficient embryos. (**A**) Morphology of yolk sacs from E11.5 wild-type (left) and *caspase-8*$^{DED/DED}$ (right) embryos. Large vitelline blood vessels (shown by an arrowhead) are clearly observed in the wild-type, but not the *caspase-8*$^{DED/DED}$, yolk sac. (**B**) Whole-mount immunohistochemistry of yolk sacs dissected from wild-type (bottom) and *caspase-8*$^{DED/DED}$ (top) embryos. Yolk sacs prepared at E9.5 (left), E10.5 (middle) and E11.5 (right) were immunostained with an anti-PECAM-1 antibody. Regressive vessels are indicated by arrowheads. (**C** and **D**) Whole-mount immunostaining of E10.5 wild-type (left) and *caspase-8*$^{DED/DED}$ (right) embryos. Embryos proper were immunostained with anti-PECAM-1 antibody as described in Materials and Methods. (**E**) Histological analysis of yolk sacs dissected from wild-type (left) and *caspase-8*$^{DED/DED}$ (right) embryos at E11.5. Yolk sac sections were stained with hematoxylin and eosin. A vessel containing blood cells and a vessel lacking blood cells are shown by an arrow and an arrowhead, respectively. Blood cells were detected in only a few vessels of each E11.5 mutant yolk sac. Abbreviations: WT, wild-type; *−/−*, *caspase-8*$^{DED/DED}$

analysis of the vasculature, it was readily apparent that E11.5 mutant vessels contained far fewer blood cells than vessels of wild-type yolk sacs (Figure 3E). These results indicate that caspase-8 is necessary for normal maturation of the yolk sac primary capillary plexus into the more mature tree-like hierarchy of vessels, and probably for development of blood cells.

On the other hand, whole-mount immunostaining of E10.5 embryos with anti-PECAM-1 antibody revealed no differences between the vascular systems of wild-type and *caspase-8*$^{DED/DED}$ embryos proper (Figure 3C, D). A similar branched network of blood vessels was observed in both wild-type and mutant embryos. These results indicate that caspase-8 activation is required for angiogenesis only in the extraembryonic yolk sac.

Cardiac rupture in *caspase-8*$^{DED/DED}$ mutant embryos

To learn more about the defects in *caspase-8*$^{DED/DED}$ embryos associated with abdominal hemorrhage, detailed histological analyses were performed on E10.5−11.5 embryos. As shown in Figure 4A and B, we confirmed that the abdominal hemorrhage was the result of an efflux of blood cells into the pericardial cavity, and that the main muscular framework of the heart had undergone lysis. By terminal

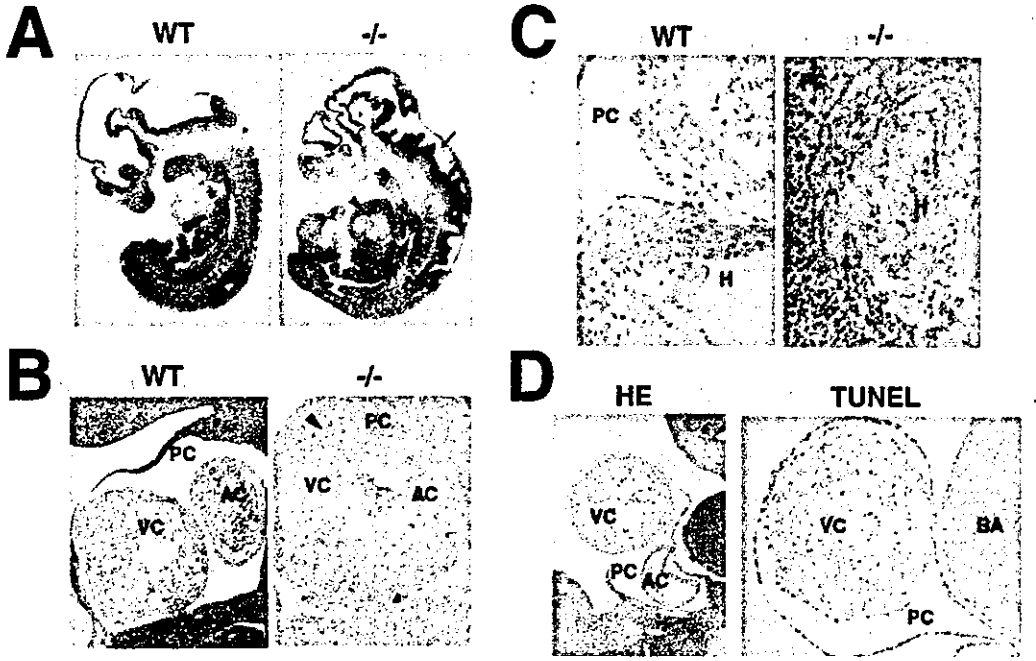

Figure 4 Histological analysis of heart tissue from caspase-8-deficient mice. (A and B) Hematoxylin and eosin (HE) staining of sagittal sections of E11.5 wild-type (left) and *caspase-8*$^{DED/DED}$ (right) embryos. Hemorrhage is shown by arrowheads in photographs of whole body (A) and pericardial cavity and heart (B). The arrow shows the neural tube, which developed irregularly, in the *caspase-8*$^{DED/DED}$embryo. (C) TUNEL staining of hearts from E11.5 wild-type (left) and *caspase-8*$^{DED/DED}$ (right) embryos. TUNEL-positive cells (colored brown) are apoptotic. (D) HE and TUNEL staining of the E10.5 *caspase-8*$^{DED/DED}$ embryo. Sagittal sections were stained with hematoxylin and eosin (left) and analyzed by TUNEL staining (right). No TUNEL-positive cells were observed in the *caspase-8*$^{DED/DED}$ heart. Abbreviations: WT, wild-type; −/−, *caspase-8*$^{DED/DED}$; H, heart; PC, pericardial cavity; AC, atrial chamber; VC, ventricular chamber; BA, branchial arch

deoxynucleotidyl transferase-mediated dUTP-digoxigenin nick-end labeling (TUNEL) staining of *caspase-8*$^{DED/DED}$ E11.5 embryos, we found that the lytic change was due to apoptosis of cardiomyocytes (Figure 4C). Interestingly, neither cardiac rupture nor cardiomyocyte apoptosis was observed at E10.5 (Figure 4D). In addition, no apoptosis was observed in E11.5 *caspase-8*$^{DED/DED}$ embryos in tissues other than the heart (data not shown). Thus, it appears that this malformation event occurs during heart development between E10.5 and E11.5, subsequent to the appearance of yolk sac defects. We assume that cardiac rupture secondary to cardiomyocyte apoptosis is the major reason for embryonic lethality in caspase-8-deficient mice.

Neural tube defects in *caspase-8*$^{DED/DED}$ mutant embryos

Another aberrant phenotype observed in the mutants was a defect in the neural tube. As shown in Figure 5A, the neural tubes of E11.5 *caspase-8*$^{DED/DED}$ embryos displayed a kink-like irregular pattern as compared with E10.5 embryos. These observations were confirmed by histological analysis (Figure 4). To further analyze the neural tube defect, we examined the expression of neurogenic and neuronal markers by *in situ* hybridization and immunohistochemical analyses (Figure 5B–E). Although *caspase-8*$^{DED/DED}$ and wild-type embryos exhibited similar expression patterns at E10.5, the former exhibited altered patterns by E11.5. The ventricular zone became narrower in the mutant, and expression of neurogenic cell markers in that region (Pax6, Mash1 and Neurogenin-2) was diminished relative to the wild-type. In addition, though some neuronal proteins (β-tubulin, neurofilament, and Islet-1) remained at wild-type levels, transcripts of other neuronal markers (Islet-2, Chox-10, En1, and Evx1) disappeared or were dramatically reduced in the mutant neural tube. Surprisingly, we were unable to detect massive apoptotic cells in the neural tube of mutant embryos (data not shown), in contrast with their prominence in the heart (Figure 4C). Based on these observations, we conclude that loss of function of caspase-8 affects neural tube development between E10.5 and E11.5.

Rescue of *caspase-8*$^{DED/DED}$ mutant phenotypes in whole-embryo culture

It is difficult to distinguish whether the abnormal cardiomyocyte apoptosis is a direct result of caspase-8-deficiency or a secondary effect of cells lacking the physiological action of caspase-8. To understand the effect of the caspase-8-deficiency in the heart, we performed whole-embryo culture

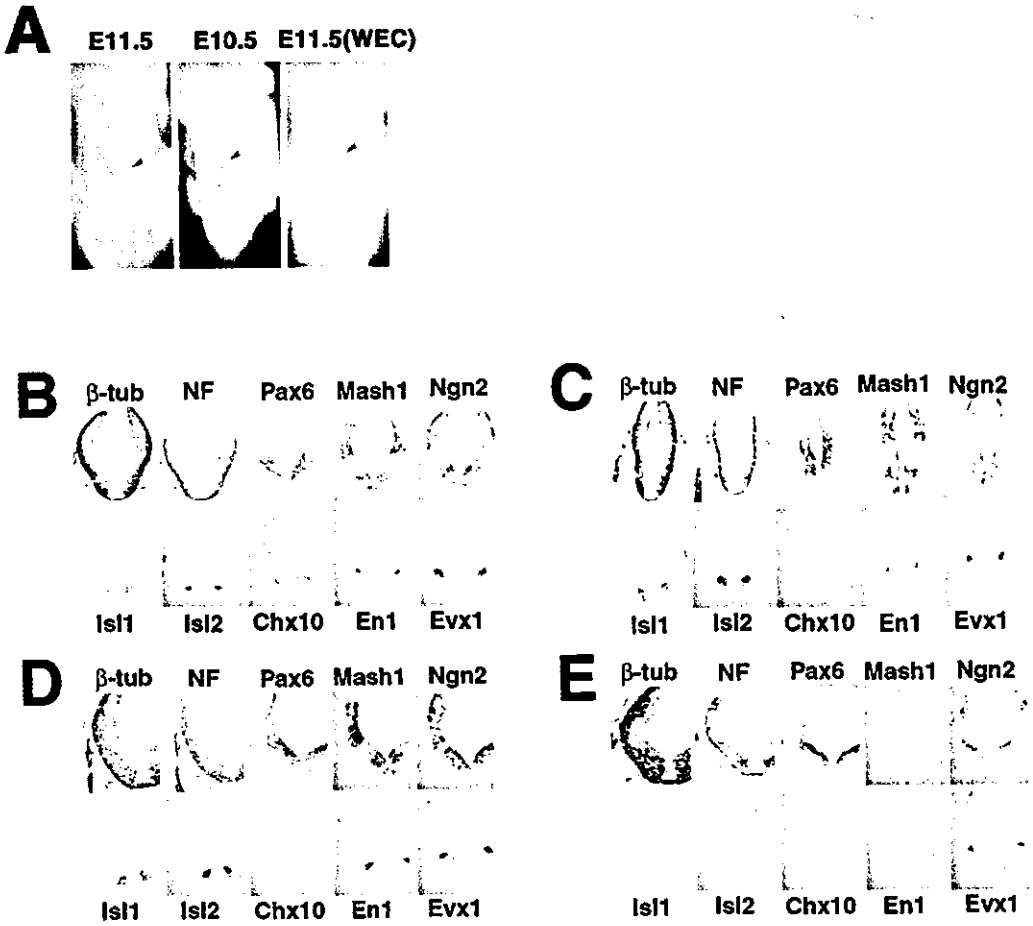

Figure 5 Morphological and neuron-specific gene expression analyses of the caspase-8-deficient neural tube. (**A**) Morphology of the neural tubes in *caspase-8*$^{DED/DED}$ embryos. Neural tube kinks were observed in the embryo dissected at E11.5 (left), but not at E10.5 (middle) or in E11.5 embryo after whole-embryo culture (WEC) (right). Neural tubes are indicated by arrowheads. (**B–E**) Immunohistochemistry and *in situ* hybridization of neural tubes from wild-type (**B** and **D**) and *caspase-8*$^{DED/DED}$ (**C** and **E**) embryos. Transverse sections of hindbrain neural tube prepared at E10.5 (**B** and **C**) and E11.5 (**D** and **E**) were examined with antibodies against β-tubulin (β-tub), neurofilament (NF), Pax6 and Islet-1 (Isl1) and with RNA probes for Islet-2 (Isl2), Chox-10 (Chx10), En1, Evx1, Mash1 and Neurogenin-2 (Ngn2) as described in Materials and Methods

of *caspase-8*$^{DED/DED}$ mutant embryos and their littermates during E10.5-E11.5. It has been shown that this whole-embryo culture system mimics the *in vivo* situation during E8-E12.[28] If caspase-8-deficiency acts in a cell-autonomous manner in cardiomyocytes, the mutant phenotype would be reproducible by *ex vivo* culture. Unexpectedly, cardiac rupture was no longer observed in *caspase-8*$^{DED/DED}$ embryos after 24 hours cultivation, which grew as well as wild-type embryos from 34–38 somites to 45–50 somites comparable to E11.5 normal embryos *in vivo* (Figure 6A). Histological analysis of cultured *caspase-8*$^{DED/DED}$embryos also showed normal heart development (Figure 6B). Myocardial trabeculation developed normally in *caspase-8*$^{DED/DED}$ hearts during culture. In addition, apoptotic myocytes were not observed in the heart by TUNEL staining, although a few apoptotic cells were detected in other tissues including the midgut. These results indicate that caspase-8 is not directly involved in myocyte survival by itself, and we emphasize that the heart defect occurs as a secondary result.

Interestingly, whole-embryo culture of *caspase-8*$^{DED/DED}$ embryos also resulted in normalization of neural tube formation, as neural tube kinks disappeared upon whole-embryo culture (Figure 5A). Normal development of the neural tube of the *caspase-8*$^{DED/DED}$ embryo was confirmed by histological observation (Figure 6A). Furthermore, no differences were detectable in the expression patterns of neurogenic and neuronal markers between wild-type and *caspase-8*$^{DED/DED}$ embryos by *in situ* hybridization analysis (Figure 6C). Expression of both neurogenic (Mash1 and Neurogenin-2) and neuronal (En1 and Evx1) markers was

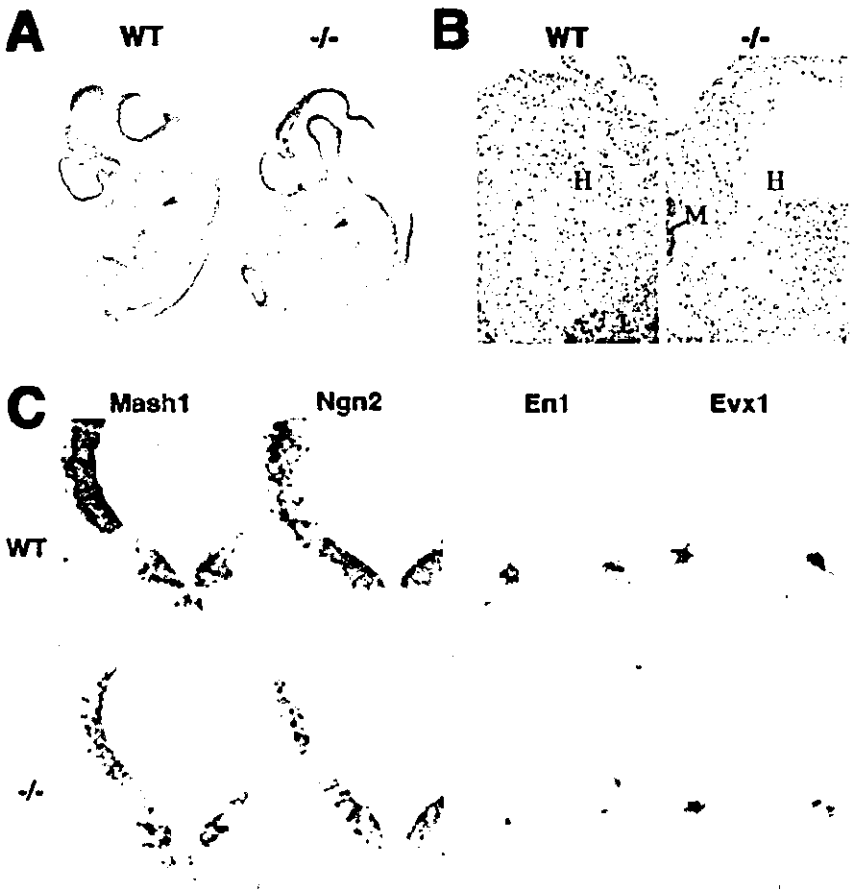

Figure 6 Recovery of caspase-8-deficient embryos by *ex vivo* whole-embryo culture. (**A**) Histology of wild-type (left) and *caspase-8*$^{DED/DED}$(right) embryos cultured during E10.5–E11.5. Sagittal sections of embryos (45–50 somites) grown up from E10.5 embryos (34–38 somites) during culture were stained with hematoxylin and eosin. The hearts are indicated by arrowheads. (**B**) TUNEL staining of hearts from wild-type (left) and *caspase-8*$^{DED/DED}$ (right) embryos after whole-embryo culture. TUNEL-positive cells (colored brown) were not detected in the heart, but were detected in other tissues such as liver and midgut of both wild-type and *caspase-8*$^{DED/DED}$ embryos. (**C**) *In situ* hybridization of neural tubes from wild-type (top) and *caspase-8*$^{DED/DED}$ (bottom) embryos after culture. Transverse sections of hindbrain tube were examined with RNA probes for Mash1, Neurogenin-2 (Ngn2), En1 and Evx1. Abbreviations: WT, wild-type; −/−, *caspase-8*$^{DED/DED}$; H, heart; L, liver; M, midgut

detected in mutant as well as wild-type embryos. Thus, both major defects could be rescued by whole-embryo culture.

Discussion

In this study, we generated caspase-8-deficient mice devoid of proteolytic function, but expressing the DED domains of caspase-8, by targeted disruption using homologous recombination. Homozygous *caspase-8*$^{DED/DED}$ mice display an inappropriate vascular system formed in the yolk sac and defects in the developing neural tube as well as heart and die at E11.5, clearly indicating for the first time that protease activity of caspase-8 is necessary for angiogenesis in the yolk sac and organogenesis during embryonic development.

Importantly, these mutant phenotypes can be rescued by *ex vivo* whole-embryo culture. No cardiac rupture or neural tube kinks occurred during culture (Figure 5A and 6), clearly indicating that these abnormalities may not all represent direct effects of caspase-8 deficiency. This evidence contradicts a previous report describing the direct involvement of caspase-8, its adapter FADD and the inhibitor molecule Casper in cell growth and survival of the developing heart.[25] In our current study, however, caspase-8 protease activity, which is required for induction of apoptosis in a variety of cells, was found to be absolutely necessary for tissue formation during embryonic development. Moreover, we found that homozygous caspase-8-deficient ES cells are able to differentiate into cardiomyocytes *in vitro*, suggesting no requirement of caspase-8 for

cell growth and differentiation (data not shown). One possible explanation for the aberrant phenotypes of the mutant mice is that a factor or factors released from cells which survive inappropriately due to failure of caspase-8-mediated apoptosis are responsible for the irregular development of the heart and neural tube as a secondary effect. During whole-embryo culture, these harmful factors could be diluted in the culture medium. Therefore, we hypothesize that caspase-8 and FADD transmit a death signal used to eliminate unwanted cells and that Casper antagonizes this signal in order to effect the survival of cells required for heart development. The whole-embryo culture system will be a valuable tool for assessing this hypothesis and understanding the physiological significance of caspase-8-mediated apoptosis during development, as well as the causal relations of defects observed in our protease-deficient caspase-8 mutant mice.

During development, the process of pruning is essential for the maturation of the vascular system. The term is used to describe the loss of excess endothelial cells generated during vasculogenesis, resulting in a tree-like pattern of vasculature typical of normal angiogenesis.[29] In this study, we have shown that this remodeling process is defective in the yolk sacs of caspase-8-deficient mice (Figure 3). Interestingly, this process was normal in the embryo proper. In addition, we confirmed by immunohistochemical analysis that vessels connecting the embryo proper and the yolk sac are normally developed and contain blood cells in *caspase-8$^{DED/DED}$* embryos (data not shown). Therefore, it seems that caspase-8 is essential for extraembryonic vascularization. By RT–PCR analysis, we were able to detect caspase-8 transcripts in the yolk sacs of wild-type embryos isolated at E10.5 and E11.5 (data not shown). Furthermore, it has been shown that programmed capillary regression is accompanied by apoptosis.[30] These pieces of evidence suggest that pruning may be associated with caspase-dependent apoptosis and that caspase-8 is involved in this process.

Notch is an important molecule for controlling signal transduction and cell fate in vertebrate and invertebrate development.[31] Deficiency of Notch signaling influences organogenesis of many tissues. Interestingly, among the many defects resulting from disruption of the Notch signaling system, abnormalities of the heart, neural tube and yolk sac were observed which remarkably resemble those of our caspase-8-deficient mice.[32–34] This would suggest a potential connection between caspase-8 and the Notch signaling system. Further analysis, including an examination of the downstream molecules of the Notch signaling pathway in caspase-8-deficient mice, will be required in order to verify this potential connection.

We have demonstrated that caspase-8 is essential during mid-stage mouse embryonic development. However, the fact that caspase-8 was clearly observed in the thymus, skin and muscle of the wild-type E17 embryo (Figure 1) suggests that it may play an equally important role during the later stages of embryogenesis. Recent studies have shown that Fas transcripts are detectable in the developing thymus of E16.5 embryo,[35] and that mouse thymocytes undergo apoptosis when treated with an agonistic anti-Fas antibody.[36] In addition, deficiency of FADD resulted in abnormal development of thymocytes in the mutant mice.[24] Because the activities of FADD, Fas and caspase-8 are so closely intertwined, and because caspase-8 protein is present in the E17 thymus, it is reasonable, based on these findings, to predict an important functional role for caspase-8 in thymic development.

To understand the role of caspase-8 *in vivo*, we and another group have generated caspase-8-deficient mice and shown that caspase-8 is involved in embryonic development. However, knowledge from these knockout mice is not sufficient to fully determine the physiological role of caspase-8 in embryogenesis. Consequently, these studies raise new questions, including how caspase-8 is activated during development. As Fas-, TNFR1-, DR3-DR6- and TRAIL-deficient embryos are viable,[37–42] caspase-8 activation must occur in a manner independent of death receptors. Furthermore, it has been shown that both caspase-3- and Bid-deficient embryos displayed normal development of the heart, neural tube and yolk sac.[18,43] As these molecules are both caspase-8-specific substrates, it seems reasonable to predict the existence of another target molecule recognized by caspase-8 during embryogenesis. Clearly, the caspase-8-mediated signaling pathway, as it functions during embryonic development, requires further elucidation.

Materials and Methods

Construction of the targeting vector and establishment of caspase-8 knockout mice

A targeting vector was constructed for generating a truncated caspase-8 protein through introduction of a stop codon at exon 7 of the mouse *caspase-8* gene.[26] In brief, a 1.2-kb *Eco*RI–*Xba*I fragment of the 5′ homologous region was ligated with the stop sequence, the polyadenylation signal derived from SV40 virus and a PGK-neo resistance gene expression cassette (PGKneobpA).[44] Then, the 5-kb *Bam*HI–*Eco*RI fragment from the 3′ homologous region containing exon 8 and the MC1-diphtheria toxin A fragment gene expression cassette (DT-A)[45] were fused at the 3′ end of the vector. The targeting vector was linearized and introduced into R1 ES cells[46] by electroporation. After screening by G418 selection at 180 μg/ml for 7–10 days, four recombinants were identified from 500 ES clones by PCR analysis and confirmed by Southern blot analysis with a 5′-probe (see Figure 2).

Chimeric mice were produced from two independent *caspase-8$^{DED/+}$* ES clones by the aggregation method[46] using C57BL/6 8-cell-stage eggs and subsequent implantation into CD1 foster mothers.[47] The resulting chimeric males were mated with C57BL/6 females (SLC, Japan). Germline transmission of the mutant allele was verified by PCR and Southern blot analyses of tail DNA from offspring of C57BL/6 genetic background. The genotypes of embryos obtained by cross-mating the heterozygous *caspase-8$^{DED/+}$* mice were also confirmed by PCR and Southern blot analyses.

Southern blot analysis

Genomic DNAs isolated from ES clones were digested with the restriction enzyme *Bam*HI, electrophoresed through a 0.7% agarose